New flood frequency estimates for the largest river in Norway based on the combination of short and long time series

Kolbjørn Engeland[1], Anna Aano[1,2], Ida Steffensen[3], Eivind Støren[3,4], Øyvind Paasche[4,5]

[1]The Norwegian Water Resources and Energy Directorate, Oslo, Norway
[2]UDepartment of Geosciences, University of Oslo, Norway
[3]Department of Earth Science, University of Bergen, Norway
[4]Bjerknes Centre for Climate Research, Bergen, Norway
[5]NORCE Climate, Bergen, Norway

Correspondence to: Kolbjørn Engeland (koe@nve.no)

Abstract. The Glomma river is the largest in Norway with a catchment area of 154 450 km^2. People living near the shores of this river are frequently exposed to destructive floods that impair local cities and communities. Unfortunately, design flood predictions are hampered by uncertainty since the standard flood records are much shorter than the requested return period and also the climate is expected to change in the coming decades. Here we combine systematic- historical and paleo-information in an effort to improve flood frequency analysis and better understand potential linkages to both climate and non-climatic forcing. Specifically, we (i) compile historical flood data from the existing literature, (ii) produce high resolution X-ray fluorescence (XRF), Magnetic Susceptibility (MS) and Computed Tomography (CT) scanning data from a sediment core covering the last 10 300 years, and (iii) integrate these data sets in order to better estimate design floods and assess non-stationarities. Based on observations from Lake Flyginnsjøen, receiving sediments from Glomma only when it reaches a certain threshold, we can estimate flood frequency in a moving window of 50 years across millennia revealing that past flood frequency is non-stationary on different time scales. We observe that periods with increased flood activity (4000-2000 years ago and <1000 years ago) corresponds broadly to intervals with lower than average summer temperatures and glacier growth whereas intervals with higher than average summer temperatures and receding glaciers overlap with periods of reduced number of floods (10 000 to 4000 years ago and 2200 to 1000 years ago). The flood frequency shows significant non-stationarities within periods having increased flood activity as was the case for the 18th century, including the AD 1789 ('Stor-Ofsen') flood being the largest on record for the last 10 300 years at this site. Using the identified non-stationarities in the paleoflood record allowed us to estimate non-stationary design floods. In particular, we found that the design flood was 23% higher during the 18th century than today and that long-term trends in flood variability are intrinsically linked to the availability of snow in late spring linking climate change to adjustments in flood frequency.

Keywords: flood, lakes, extremes, paleofloods, Norway, non-stationarity.

1 Introduction

Floods are among the most widespread natural hazards on Earth. The impacts, destruction and costs associated with hazardous floods are increasing in concert with climate change and increase of economic values within areas susceptible to floods, a tendency most likely to strengthen in the decades to come (e.g. Alfieri et al., 2017; Hirabayashi et al., 2013; IPCC, 2012). In Europe, spatial flood patterns are changing both in terms of timing and magnitude (Blöschl et al., 2017, 2019) challenging us to examine new ways to interlink not only different types of data, but also flood information on different time scales. Earlier studies have shown that uncertainties can be reduced if, for instance, historical data are included in estimation of floods with long return periods (e.g. Brázdil et al., 2006a; Engeland et al., 2018; Macdonald et al., 2014; Payrastre et al., 2011; Schendel and Thongwichian, 2017; Stedinger and Cohn, 1986; Viglione et al., 2013). Here we seek to extend the possibility of using historical data by including time series of reconstructed floods based on lake sediment archives which can retain imprint of past flood activity (Gilli et al., 2013; Schillereff et al., 2014; Wilhelm et al., 2018). The ultimate goals of this exercise are to (i) reduce uncertainty associated with flood prediction and (ii) provide additional insight to flood variability on longer time scales, and thereby improve our understanding of how climate change impacts floods.

In many European countries, flood mitigation measures aim to reduce the exposure and vulnerability of the society to floods. Examples of such measures can include reservoirs, flood safe infrastructure, and land-use planning in flood-exposed areas. These mitigation measures require estimates of design floods, i.e. the flood size (typically given in m^3/s) for a specified annual exceedance probability (AEP) or return period (RP). The required design AEP or RP depends on the impact of a flood. The Norwegian building regulations (TEK17, 2018) exemplifies this. They require that buildings of particular societal value such as hospitals should be able to resist or be protected from at least a 1,000-year flood whereas normal settlements should withstand 200-year flood and storage facilities at least a 20-year flood. Design flood estimates are commonly based on analysis of the frequency and magnitudes of observed floods using measurements derived from a streamflow gauging station. Recall that for many applications, estimates of 200- up to1000-year floods are required (see Lovdata, 2010, and TEK17, 2018 for regulations in Norway). This is not a trivial task for at least two reasons. Firstly, we have limited amount of data and the estimation uncertainty for a 1000-year flood is large with only 50-100 years of data. Secondly, we plan for the future (i.e. for the life time of a construction), but in many cases it can be necessary to account for non-stationarities in floods caused by past as well as anticipated future changes in climate.

Both challenges can be addressed by using data covering longer time periods including historical data (e.g. Benson, 1950; Brázdil et al., 2006b; Macdonald et al., 2014; Schendel and Thongwichian, 2017; Viglione et al., 2013) and/or paleoflood data (e.g. Benito and O'Connor, 2013). The fact that sediment deposits can be unambiguous evidence of past floods is documented in many studies since 1880 AD (Bretz, 1929; Dana, 1882; Tarr, 1892), and an early example of how to estimate discharge associated with giant paleofloods can be found in Baker (1973) whereas paleoflood hydrology as a concept and terminology was first introduced by Kochel and Baker (1982).

In order to include information about past floods in flood frequency analysis, it is necessary to estimate the flood sizes in m^3/s. A successful approach for assessing the stage and the volumes for paleofloods is to use slack-water deposits along river canyons (e.g. Baker, 1987, 2008; Benito and O'Connor, 2013; Benito and Thorndycraft, 2005). Following this approach, water level during floods can be deduced from the elevation of the deposits enabling hydraulic models to estimate flood volumes for specific events. During the recent 20 years, lacustrine sediments has proven to be another reliable source of paleofloods (Gilli et al., 2013; Schillereff et al., 2014; Wilhelm et al., 2018). Sediment cores retrieved from lakes that periodically receive sediments delivered by floods can be used to extend local hydrological time series spanning thousands of years. Since lake sediment archives for the most are continuous records, they can complete the snapshot information provided by flood terraces still present in the landscape or anecdotal information about historical floods.

Lakes fit for using lacustrine sediments to analyze flood frequencies are typically found where (i) flood sediments are preserved at the bottom of lakes (ii) there is a detectable on/off signal for sediments left by floods, and (iii) a distinct contrast

between flood deposits and regular background sedimentation (Gilli et al., 2013). Detection of flood layers in the cores can be based on X-ray fluorescence (XRF) scanning (e.g. Czymzik et al., 2013; Støren et al., 2016) magnetic susceptibility (MS) measurements (e.g. Støren et al., 2010), computed tomography (CT) scanning (e.g. Støren et al., 2010), or spectral reflectance and color imaging (Debret et al., 2010).

There are multiple sources for historical flood data (e.g., Brázdil et al., 2012), and depositories of historical flood data can be found in Brázdil et al. (2006a) and Kjeldsen et al. (2014). An overview over historical floods in Norway is available in Roald (2013). For quantitative analyses, it is nonetheless necessary to find evidence of historical flood stages, e.g. from flood stones or flood marks, and estimate flood discharge based on hydraulic calculations (Benito et al., 2015).

Systematic measurements of floods date back to the Common Era (CE) 1870. Historical flood information in Norway is often available back to the 17th century, there is, however, scattered information on earlier floods including one that occurred in the 1340s. This is different from paleoflood data in Norway which typically cover the Holocene period (11700 years) and extends all the way until present day. The difference in time periods covered by diverse data sources on past flooding highlights the potential of using historical- and paleo flood data to both reduce estimation uncertainty of design floods with long return periods and to assess non-stationarities in floods. The paleo- and historical flood information can be used – in combination with systematic data – to estimate design floods (see e.g. Engeland et al., 2018; Kjeldsen et al., 2014; Stedinger and Cohn, 1986). To include the paleo- and historical information in flood frequency analysis, we also need to know all floods exceeding a fixed threshold during a specified time interval. Several studies demonstrate that, given that the fixed threshold is high enough, it is adequate to know the number of floods exceeding this threshold in order to improve flood quantile estimates (Engeland et al., 2018; Martins and Stedinger, 2001; Payrastre et al., 2011; Stedinger and Cohn, 1986). A Bayesian approach to flood frequency analysis with historical- and paleodata sources was introduced by Stedinger and Cohn (1986) and Gaál et al. (2010). This approach allows, in a flexible way, the introduction of multiple fixed thresholds and data sources, and is therefore well suited for combining systematic- historical and paleo- data in a joint flood frequency analysis.

When we predict flood frequency for the future, the standard assumption is stationarity or put differently: it's assumed that the period with instrumental data is representative for the future. In many cases, when the analysis is based on flood data from a streamflow gauging station covering a limited period, it is a robust assumption (Serinaldi and Kilsby, 2015). However, in the face of expected changes in climate, it is useful to take into account the risk for floods in the future (Hanssen-Bauer et al., 2017; Lawrence, 2020; Paasche and Støren, 2014). For Norway, tailored guidelines for adaption to future flood risk are provided by the Norwegian Center for Climate Services (https://klimaservicesenter.no/) based on results from climate projection studies (Lawrence, 2020). A current practice is to use flood inundation maps where estimated future flood levels for specific return periods are shown (e.g. NVE flood zone maps, 2020; Orvedal and Pereeboom, 2014). Such maps are commonly used in land-use planning.

Since the historical- and paleodata covers much longer time periods than streamflow data, they can be an excellent source for non-stationarity in actual flood sizes and the underlying flood generating processes. One approach is to link the frequency of floods to the underlying climatic drivers (e.g. mean temperature, precipitation and large-scale circulation patterns (e.g. Gilli et al., 2013; Kjeldsen et al., 2014; Støren et al., 2012; Støren and Paasche, 2014). A major challenge when using paleo- and historical flood information, is precisely to disentangle non-stationarity in climatic drivers from non-stationarities caused by changes in land-use and/or the 'archiving processes' of the data. Changes in land-use can, for instance, be related to farming practices and timber-logging. Changes in the archiving process might be caused by changes in the perception threshold that depend on societal development (Kjeldsen et al., 2014; Macdonald and Sangster, 2017). Also changes in the river channel might limit the possibility to estimate the magnitude of paleo- and historical floods (Brázdil et al., 2011).

The primary objective of this paper is to combine systematic- historical and paleo-information in a flood frequency analysis in order to better understand and predict changes in flood frequency and magnitude for Norway's largest river, Glomma. In particular we want to explore:

- Past variability in floods as reconstructed from lake sediment cores.
- Potential non-stationarity in our new paleoflood record and its potential connection to regional climate change.
- The added value of combining systematic-, historical-, and paleo-flood data when estimating flood quantiles.
- Potential non-stationarities in design floods.

The unique contribution of this study is thus to combine three different information sources in an attempt to improve flood frequency estimations and better understand the underlying mechanisms that cause significant changes in flood variability over time.

2 Study area

2.1 Study catchment

The target site for this study is the city Elverum lying next to the river Glomma. A gauging station having an upstream catchment area of 154 450 km² (Fig. 1) is located in the city. The elevation in the catchment ranges from 180 masl at Elverum to 2178 masl at the highest mountain and is covered by forest (52 %), open areas above the timber line (27%), bogs (10 %), lakes (3%), and agricultural areas (2%). Only 0.13% is represented by urban areas. The average annual precipitation is 580 mm with the summer months being the wettest. The annual average temperature is -0.65 °C but the climate is continental. January has the coldest month with -11.2 °C whereas July is the warmest with 10 °C. The low winter temperatures result in a considerable seasonal snow cover which has a direct impact on the streamflow. Minimum flows are observed during winter (December – April) whereas the highest flows take place during the snow melt season (May – June), as shown in Fig. 2. The main flood season occurs during the snow melt season (May – June) with the rare exception of a few minor floods that arrive during the autumn season due to long duration intense rainfall.
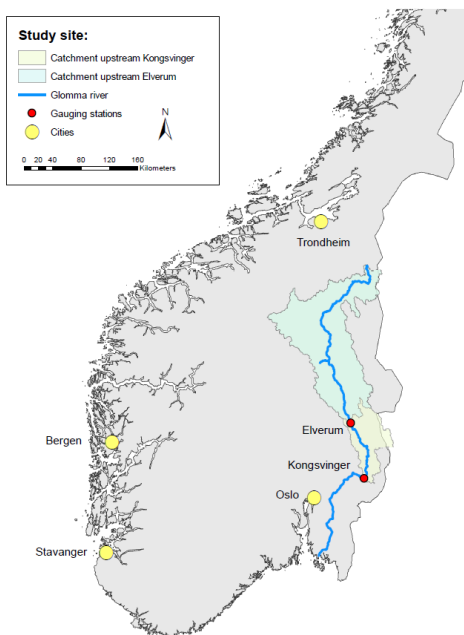
Figure 1: The location of the streamflow gauging station at Elverum used for flood frequency analysis, and the site for paleodata collection close to Kongsvinger city.

The catchment has several hydropower reservoirs with a total regulation capacity presently around 10% of the average annual runoff. The first reservoir was built in 1913, and since 1937 this and other reservoirs have resulted in decreased flood sizes (Pettersson, 2000). The monthly flows during winter has increased and most flood peaks have decreased after 1937 (Fig. 2). The catchment has undergone noteworthy land-use changes during the last 400 years. In the 17-19th century, the forest

areas were reduced due to mining, timber export and farming practices. Since the beginning of the 20th century, the forest covered areas have increased slightly whereas the timber volume has increased substantially mainly due to farming and forestry practices e.g. reduced grassing of domestic livestock and forestation, (Grønlund et al., 1999).
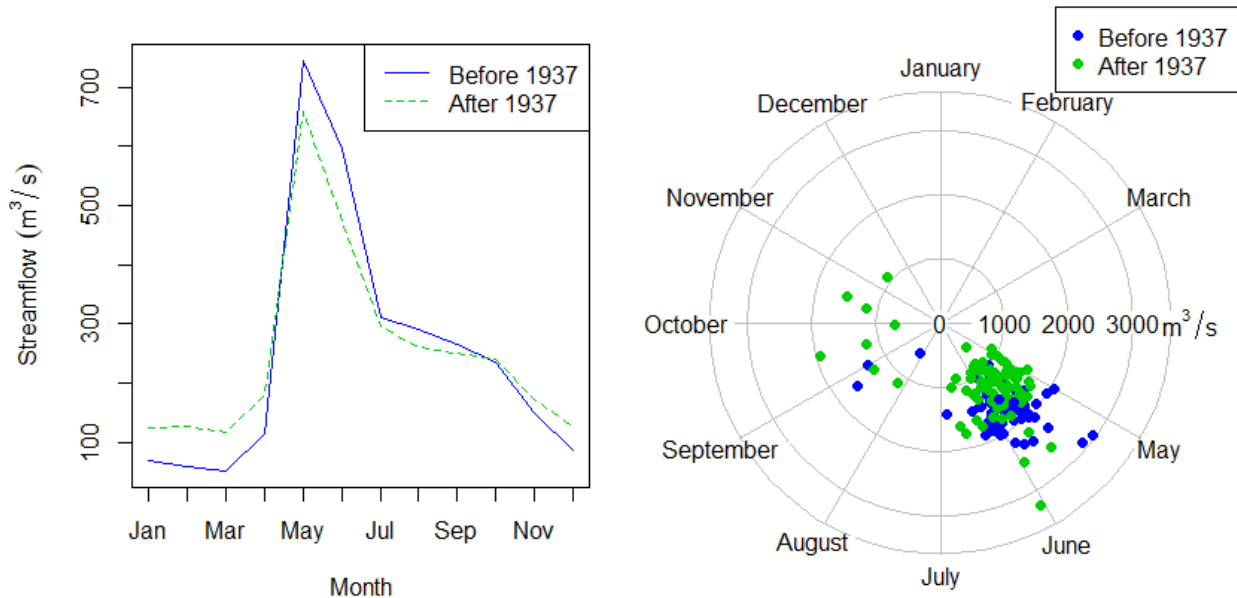
Figure 2: Seasonality of Glomma's monthly streamflow (left) and annual maximum floods (right) at Elverum. The dampening of floods after 1937 is explained by up-stream dam-building.

2.2 Study site for paleodata

To establish a flood record covering most of the Holocene (<11 700 years, Walker et al. (2009)), two sediment cores were retrieved at 16 m water depth from Flyginnsjøen (UTM: 33V 0337459 6670202) located close to Kongsvinger, around 80 km south of Elverum as the crow flies (Fig. 1). A detailed map of the study area is shown in Fig.3 and conceptual model of the lakes involved, flood water levels, thresholds and flood pathways are shown in Fig. 4. During normal conditions, water flows from Tarven and Vingersjøen (catchment area 72.0 km^2) into Glomma. When the streamflow in Glomma exceeds 1500 m^3/s, the flow direction reverses, and around 1-2 % of the water flows from Glomma and over to Vingersjøen and further into Tarven, Flyginnsjøen, leaves the Glomma catchments and follows the river Vrangselva across the border to Sweden (Pettersson, 2001). These bifurcation events enable flood water from Glomma to reach Flyginnsjøen where part of the suspended sediment load is deposited. This is in stark contrast to 'normal conditions' for the lake, when the minerogenic sediment delivery is marginal compared to the organic material, as outlined below. The repeated increase in discharge during floods, remobilize readily available sediments – originating mainly from the last deglaciation – and allow for the subsequent deposition of fine-grained minerogenic material. Bathymetric map of Lake Flyginnsjøen and the coring sites which were chosen at the deepest part of the lake, close to the inlet is shown in Fig. 5. Note that the inlet during bifurcation events is only around 30 meters away from the permanent inlet. For addition details about the study site, and its surroundings, see the master theses by Aano (2017), Follestad (2014), and Steffensen (2014).
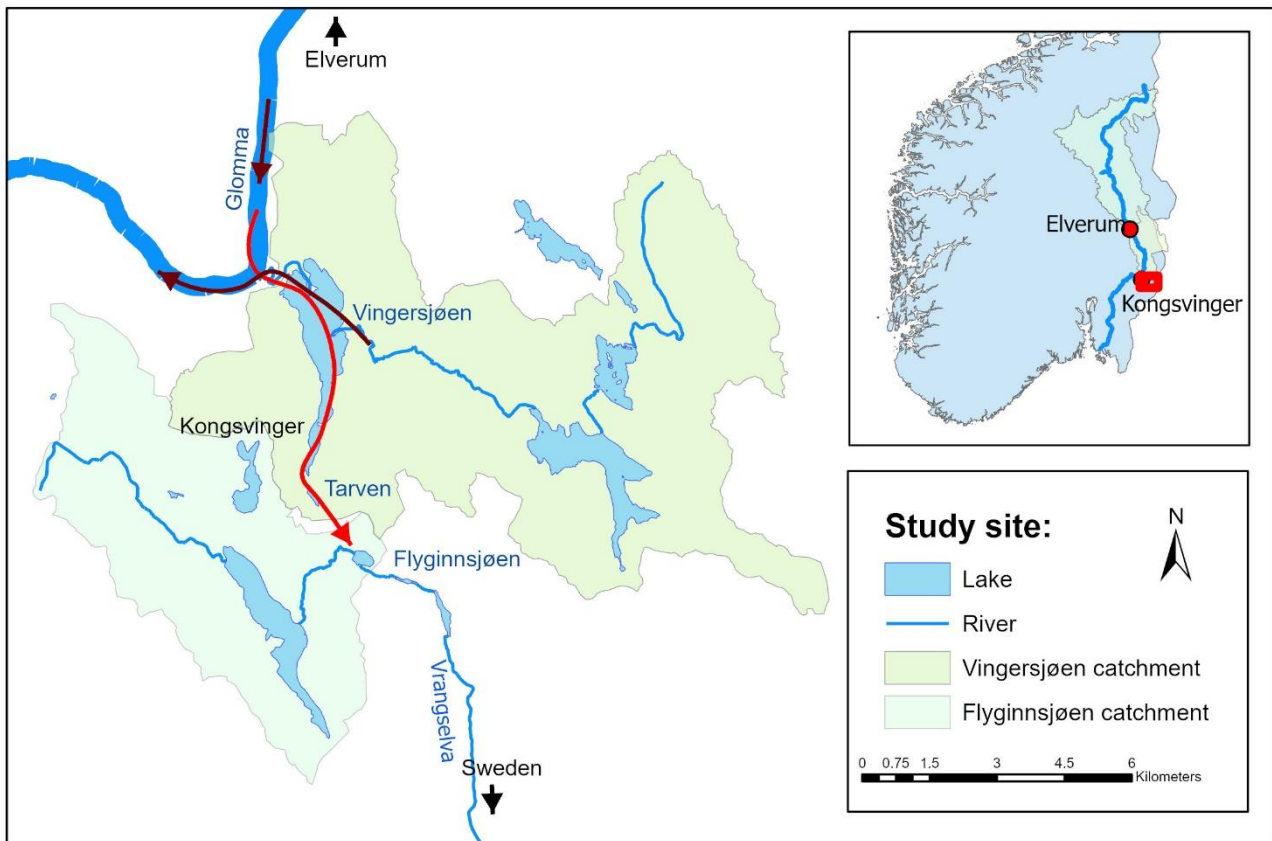
5

Areal photo: © Norwegian Mapping Authority, Geovekst and the municipalities, Oslo-Østlandet 2016

Figure 3: Study site for the paleodata. Map: The sediment cores were extracted from lake Flyginnsjøen. The green arrows indicate the flow direction under normal conditions, whereas the dark red arrow shows the flow direction whenever there is a flood that exceeds 1500 m^3/s and bifurcation occurs. Left areal photo: The river between Vingersjøen and Glomma. Under normal conditions the water flows from Vingersjøen into Glomma. Right areal photo: The flood path from Tarven to Flyginnsjøen during bifurcation events is indicated with red dots. Areal photo: © Norwegian Mapping Authority, Geovekst and the municipalities, Oslo-Østlandet 2016.
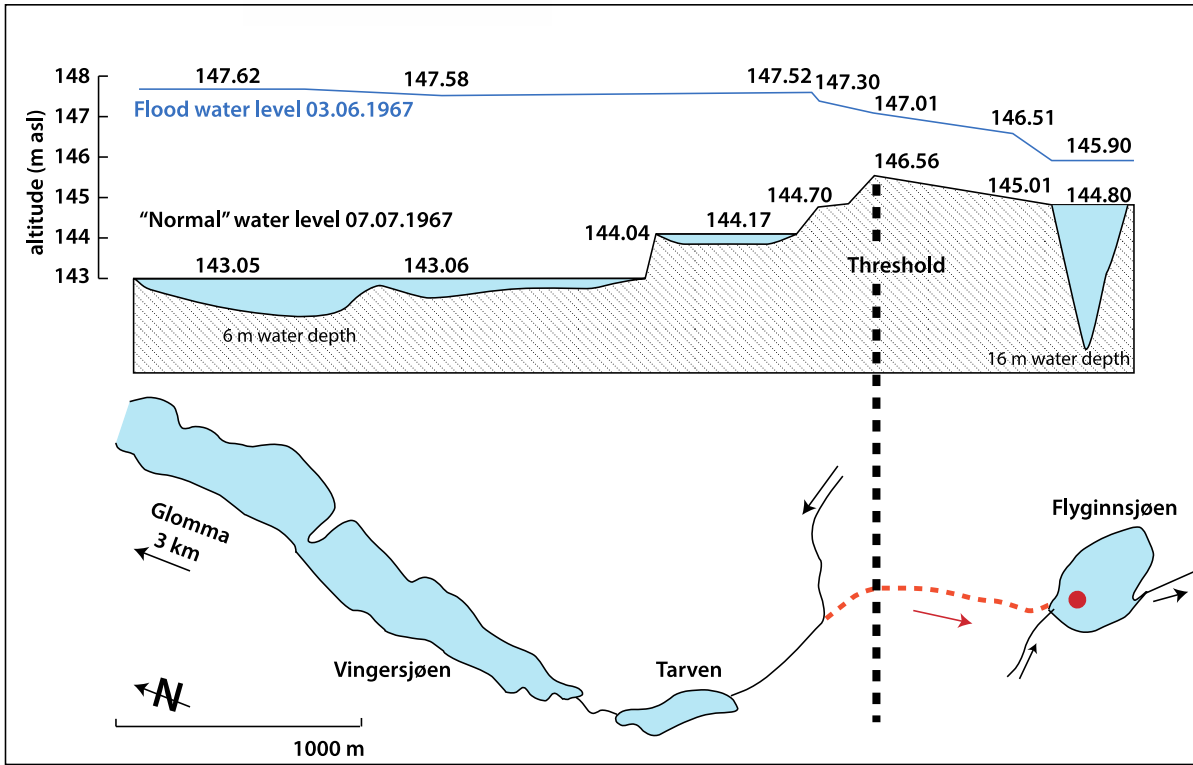
Figure 4: Schematic model of the lakes involved, flood water levels, thresholds and flood pathways (after Hegge, 1968). The example shows observed water level exceeding the threshold during the flood in 1967 (2533 m³/s), and the normal water level approx. one month after the flood event. The dotted red line and arrow show the bifurcation over the threshold, and the red point marks the coring site in Flyginnsjøen. Note that the inlet during bifurcation events is only around 30 meters away from the permanent inlet.
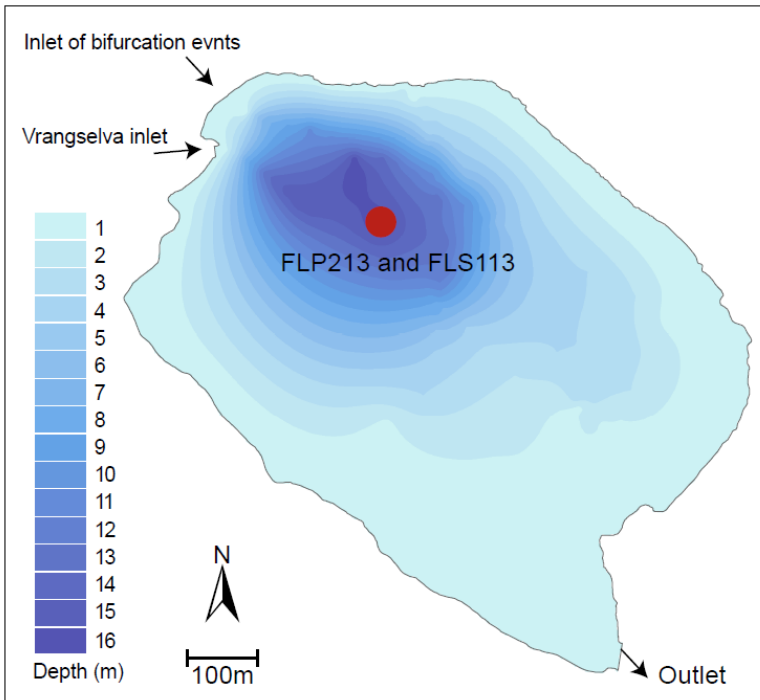
Figure 5. Bathymetric map of Lake Flyginnsjøen and the coring sites which were chosen at the deepest part of the lake, close to the inlet. Note that the inlet during bifurcation events is only around 30 meters away from the permanent inlet.

3 Data sources and Methodology-

3.1 Systematic flood data

Annual maximum flood at Elverum (station number 2.604) for the period 1872-1936 was used for the flood frequency analysis. For this period, we assumed that the flood data were not significantly affected by river regulations (Pettersson, 2000). The mean annual flood for the period 1937-2019 it is 1362 m^3/s. A Wilcoxon test indicates that the difference in mean value is significant with a p-value < 0.01 for the zero-hypothesis (i.e. no difference in mean values between the two periods). The modern observations are shown in Fig. 6 together with the known historical floods as well as annual maxima daily floods from the period after 1937, when we observe a minor decrease in average flood size after 1937.
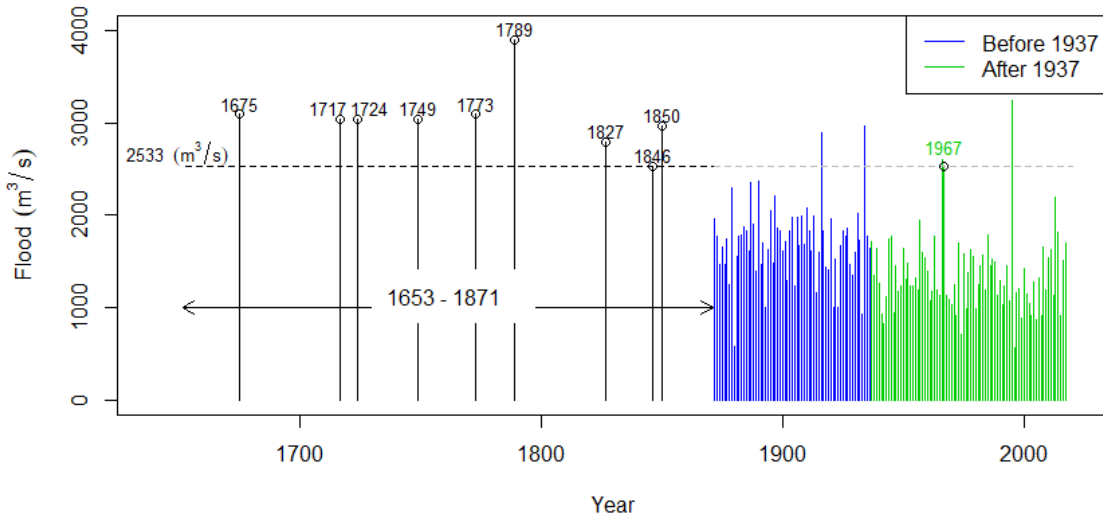

Figure 6: Systematic and historical flood data at Elverum. The systematic data from 1872 – 1936 were used for flood frequency analysis. After 1937, the floods are dampend by river regulations. The flood in 1967 reached 2533 m^3/s and was used as a threshold for the historical floods. The period for historical floods lasted from 1653-1871. The CE 1789 flood known as *Stor-Ofsen* in Norway stand out in this record.

3.2 Historical flood data

Historical flood information back to 1675 is available as water levels marked at a flood stone in Elverum, located close to Klokkerfossen ('fossen' meaning waterfall) at the Norwegian Forest Museum (Fig. 7 and Table 1-2). Table 1 lists the water levels and discharges for floods exceeding the 1967 flood are highlighted on the flood stone which was erected in 1968. The water levels were carved into the stone in 1969 based on recommendations from NVE (Hegge, 1969); the 1995 flood was added later. There is another flood stone nearby at Grindalen (also shown in Fig. 7). It was erected as early as in 1792 in order to remember the floods of 1773 and 1789, which were large indeed.

The flood stone at Grindalen is 2 km upstream the flood stone at Klokkerfossen with the streamflow gauging station at Elverum in the middle. A waterfall at Klokkerfossen is the controlling profile for the water levels at all three locations. Hegge (1969) developed relationships between water levels at the Elverum gauging station and the flood stone at Klokkerfossen shown here in Table 1. The water levels at Elverum gauging stations were transformed to discharges by using the local rating curve, which assumes that the river profile has been relatively stable since CE 1675. In this study, we included all floods exceeding the observed 1967 flood peak at 2533 m^3/s in the flood frequency analysis. By following this approach, we are confident that we only included information about all floods exceeding a specific flood level.

Table 2 summarizes the available historic information and important sources for these floods. The floods in 1675, 1717, and 1749 are all described in Finne-Grønn (1921) and Otnes (1982) whereas information for the flood mark in 1724 is not found in any written source. Detailed information about water levels for floods prior to 1773 were estimated in the absence of historical data. The water levels in 1773, 1789, 1827 and 1846 are all engraved in the flood stone in Grinsdalen and employed

here as a basis for calculating the water level at the Elverum gauging station and also for the flood stone at Klokkerfossen. Having said that, we still included all flood water levels listed in Hegge (1969). More information about historical flood of the Glomma River and at Elverum is provided by Finne-Grønn (1921), Otnes (1982), and Roald (2013). During the period 1675 to 1870, we see that 8 floods exceeded the observed 1967 flood peak at 2533 m³/s. The 18th century has a large number of floods at this location. All floods occurred in late May with the notable exception of *Stor-Ofsen* in 1789 which occurred in late July.

The largest historical flood in this region was *Stor-Ofsen* which took place in 22-23 July 1789 when peak discharge reached 3900 m³/s at Elverum (GLB, 1947) being only slightly smaller than our estimate (see Table 1). Numerous catchments in eastern Norway flooded at the time resulting in 61 fatalities, destruction of infrastructure, farms and crops. The economic losses were extraordinary and in the aftermath of the flood, around 1500 farms got tax reduction (Otnes, 1982).

Table 1: Water levels at Elverum gauging station and at the flood monument from Hegge (1969). The various streamflow peaks are constructed based on the rating curve at the gauging station 2.119 and rating curve period 1881-1970. The large floods in 1966, 1967 and 1995 were not included in this study.

Date	Height – gauging station (m)	Height – flood monument (m)	Streamflow (m³/s) Peaks
28.05.1675	4.50	3.35	3141
24.05.1717	4.30	3.22	2963
17.21.1724	4.25	3.19	2919
24.05.1749	4.20	3.16	2875
30.05.1773	4.55	3.38	3187
22.07.1789	5.35	3.86	3944
27.05.1827	4.04	3.06	2736
24.05.1846	3.87	2.95	2592
25.05.1850	4.33	3.24	2989
11.05.1916	4.30	3.22	*2892*
08.05.1934	4.36	3.26	*2963*
20.05.1966	3.90	2.97	*2600*
02.06.1967	3.87	2.95	*2533*
02.06.1995	---	---	*3238*

Table 2 Information about large historical floods at Elverum.

| Date	Information	Source
28.05.1675	Large flood in Elverum used as a reference for later floods.	Finne-Grønn (1921) Otnes (1982)
24.05.1717	The largest flood since 1675	Finne-Grønn (1921) Otnes(1982)
1724	No information found	
24.05.1749	Large amounts of snow during winter. The flood was smaller than in 1675 and similar to the floods in 1717 and 1724. The flood peaked around 12:00.	Finne-Grønn (1921) Kvernmoen and Kvernmoen(1921)
29-30.05.1773	Highest flood in man's memory and higher than in 1675. The whole village flooded. Marked at flood stone in Grindalen	Finne-Grønn (1921) Kvernmoen and Kvernmoen(1921)
22-24.07.1789	The flood peaked between 22:00 and 24:00 the whole village at Elverum destroyed. Marked at flood stone in Grindalen.	GLB (1947)
27.05.1827	2.5 alen (156 m) lower than 1789 and 0.5 alen (31.3 cm) lower than 1773. Almost the whole village was flooded. Marked at flood stone in Grindalen.	Otnes (1982)
26.05.1846	Marked at flood stone in Grindalen.	Roald (2013)
24-26.05.1850	Marked at flood stone in Grindalen.	Roald (2013)
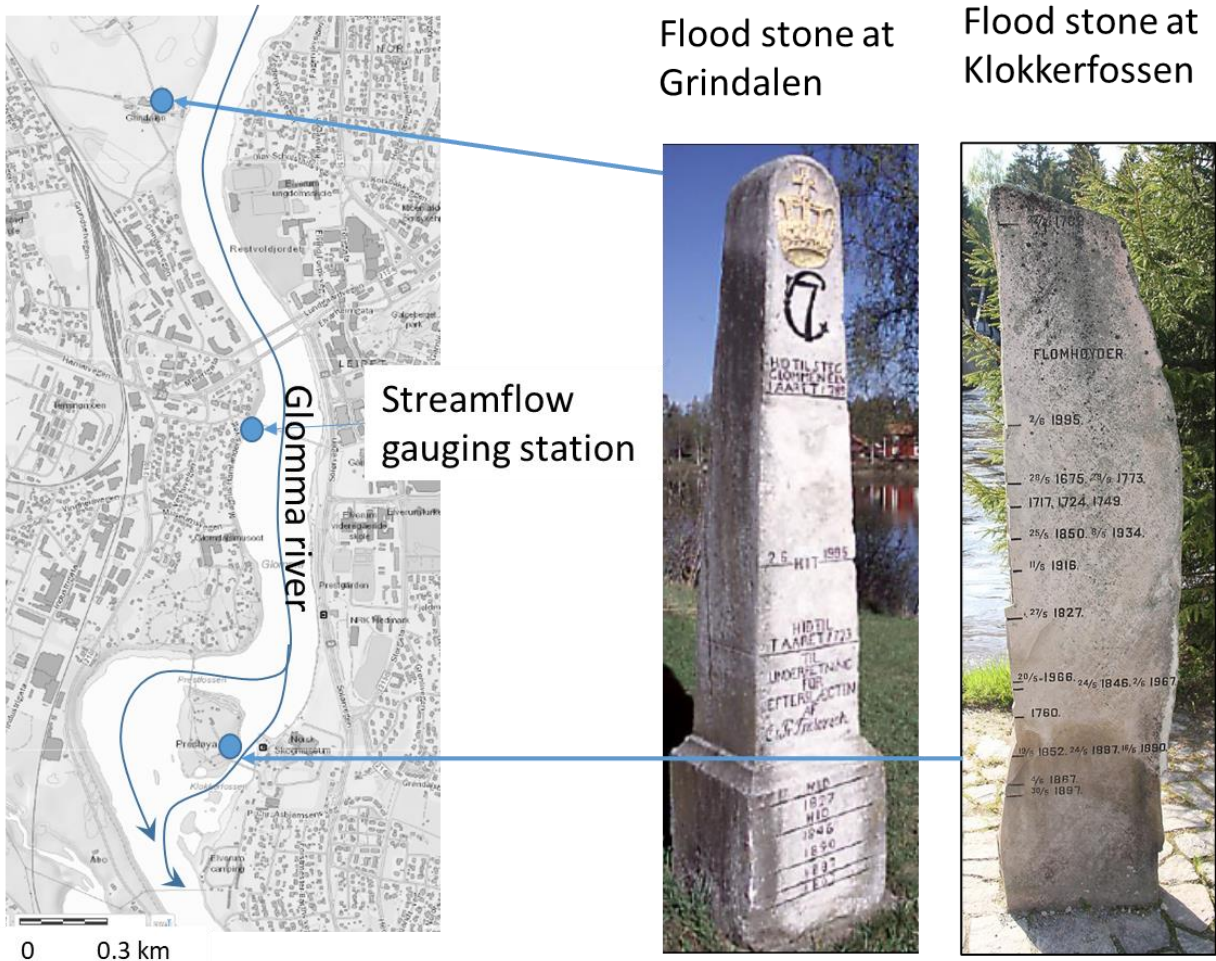
Figure 7: Map on the left shows the locations of the flood stones and the gauging station at Elverum (left). Pictures to the right shows the flood monuments at Grindalen (middle, photo: N.R. Sælthun) and Klokkerfossen at the Norwegian forest museum (right, photo: Ø. Holmstad).

Prior to *Stor-Ofsen*, there was a substantial amount of snow in the mountains, deep soil frost, and rainfall that had saturated the soil. During the actual flood event, warm and humid air masses from the southeast were blocked by colder air masses in the north-west, resulting in high rainfall over the entire region. The rainfall intensity peaked on the 22 July. The flood started on 21 July in small brooks and culminated the following day (Østmoe, 1985). The main rivers at the bottom of the valleys rose to unprecedented levels and the flood was also accompanied by numerous landslides. The water levels of this flood are known from several markings cut into rocks, and many flood levels have later been transferred to monuments erected at locations near the major rivers (Engeland et al., 2018; Finne-Grønn, 1921; Otnes, 1982; Roald, 2013).

3.2.1 Bifurcation events

Descriptions of bifurcation events and lists of estimated flow volumes in Glomma at Kongsvinger are found in Aano (2017), Pettersson (2001), Hegge (1968), and Reusch (1903). From 1851 to 2013, 79 events in 77 different years were recorded. In 1957 and 1987 there were bifurcation events both in the spring and in the autumn; 4 of the 79 events occurred during the autumn. For the interval between 1953-2013, the same period that is covered by FLS113, there were 22 bifurcation events. The transferred volume for the period 1851-2013 is presented in Fig. 8. The five years with the largest transferred volumes are 1916, 1934 1966, 1967 and 1995 with corresponding peak floods at Elverum yielding 2892, 2963, 2600, 2533, and 3238 m^3/s, respectively. Note that there is a strong statistical correlation (rsq=0.94) between transferred volume and the maximum transferred discharge. In addition to actual discharge of the individual floods, the duration of each bifurcation event determines

the total volume. The estimated peak bifurcation discharge in 1995 was substantially smaller than the estimate for 1916, despite the fact that the water level in Glomma was somewhat higher in 1995 (Pettersson, 2001). Possible explanations for this minor discrepancy are that increased vegetation and/or a local road bridge has reduced the capacity of the intermittent water course. The number of events has decreased since around 1930, mainly due to construction of hydropower reservoirs.
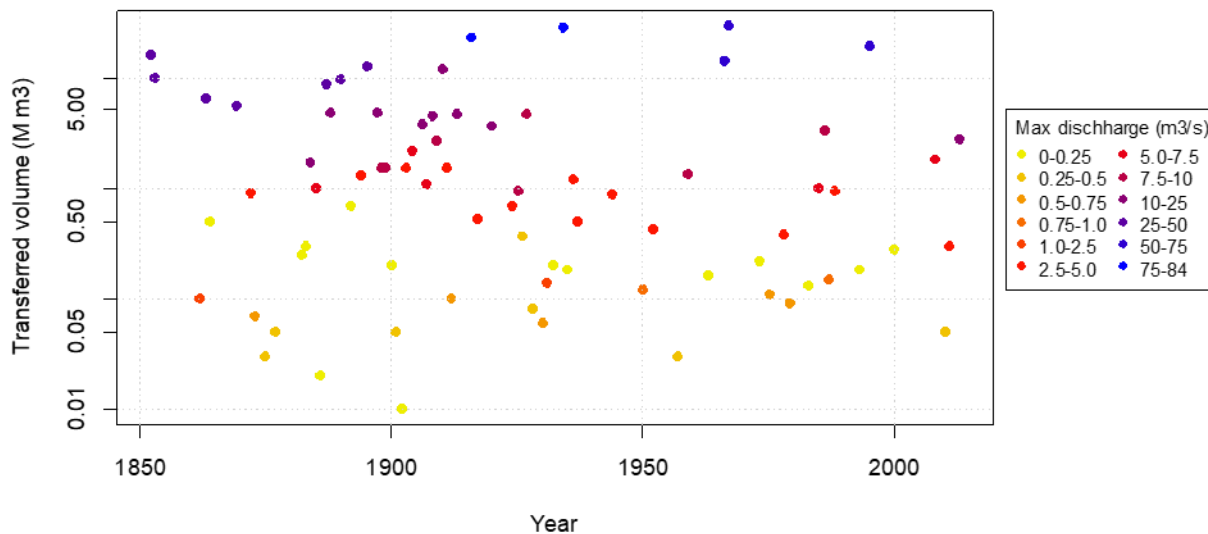
Figure 8: Transferred volume (M m^3/s) and maximum discharge (m^3/s) indicated by color for bifurcation events at Kongsvinger. Estimates are obtained from Aano (2017), Pettersson (2001), Hegge (1968), and Reusch (1903).

3.3 Paleohydrological flood data from lakes

3.3.1 Identification of sediment layers

Two sediment cores were retrieved from Flyginnsjøen in 2013 (see Sect. 2.2). Coring sites shown in Fig. 5 were selected were chosen at the deepest part of the lake based on a bathymetric survey of the lake using a Garmin Fishfinder echo sounder. A 516 cm long sediment cores were retrieved using a 110 mm diameter piston corer (FLP213) (Nesje, 1992). Since the piston corer may disturb sediment layers in the upper 15-20 cm an HTH gravity corer (FLS113) (Renberg and Hansson, 2008) was used to retrieve a 18 cm core of the youngest sediments. Samples of 1 cm^3 were extracted at 0.5 cm intervals from the sediment cores, dried overnight at 105 ºC, and weighed to measure dry-bulk density (DBD) (Blake and Hartge, 1986). The same samples were subsequently burned at 550ºC to measure the weight loss-on-ignition (LOI) as an estimate of the organic matter content (Dean, 1974). Geochemical properties of the sediment cores were measured using a Cox Analytics ITRAX XRF core scanner at 200 μm resolution, running a Cr X-ray tube at 30 kV and 45mA for 10 sec. measurements at each step. XRF measurements were normalized against total scatter (incoherent and coherent) to reduce potential influence of water content. Images of the split core surface was also captured by the ITRAX core scanner, and 8-bit (255 values) Black & White (BW) values were obtained from a 75 pixel wide average along the length of the core at 200 μm resolution using Image J software. A ProCon Alpha Core Computed Tomography (CT) scanner running at 100 kV, 200 mA for 250 ms was used to generate 3D X-ray imagery of FLS113 with a voxel resolution of 80 μm. CT data was reconstructed using ring-artefact and median filter in the Volex CT Offline software (ProCon X-ray gmbh), and visualized in Avizo Fire 9.1 (FEI) software. The CT data is given as 16-bit (65636 values) grayscale values, interpreted to indicate relative densities due to minimal photoelectric effect at 100 kV (Wellington and Vinegar, 1987) and extracted at 80 μm resolution through a centreline of the FLS113 sediment core. MS was measured on the surface of the split sediment cores at 2 mm sample intervals with a Bartington MS2E point sensor using the CoreSusc MkIII core scanner.

The area between Vingersjøen and Flyginnsjøen (Fig. 4) is rich in glaciofluvial deposits easily remobilized whenever floods occur. Bifurcation events in Glomma causes precisely such a fundamental change in the erosion regime in this area, causing river-flooding in a normally dry area (see Sect. 3.2.1). The following calculations and interpretations are thus based on the assumption that bifurcations events can be recorded as marked increase in minerogenic input to lake Flyginnsjøen, redeposited from the pre-existing glaciofluvial deposits in the catchment.

To quantify the frequency of such events a local peak detection algorithm was applied on parameters sensitive to changes in minerogenic input. Flood deposits was defined as peaks in the measured parameters where (*i*) the measured concentration is higher than the two surrounding values, (*ii*) the difference between the peak and the lowest value within a specified time window (*w*) exceeds a specified threshold h_1 and, (*iii*) the difference between tThe time lag between succeeding peak should beby at least 9 months. We chose a minimum 9-month time lag between two flood events since this catchment has one major flood event per year, typically occurring in May/June. For locations with more frequent floods, a smaller time lag could be more appropriate.

To produce a Holocene flood record based on the sediment cores from Flyginnsjøen depth in core was transformed to time using Bacon age-depth modelling software (Blaauw and Christeny, 2011) (see Sect. 4.1.1), and frequency of events in 50-year moving window was quantified. In order test to what extent the lake sediment records reproduce modern and historical observations, identified flood layers was compared to with instrumental streamflow data.

3.4 Flood frequency modelling

3.4.1 Stationary flood frequency modelling

A Generalized Extreme Value (GEV) distribution was invoked to establish a flood frequency model for floods at Elverum. The GEV distribution is shown to be a limiting distribution for block maxima (Embrechts et al., 1997; Fisher and Tippett, 1928; Gnedenko, 1943):

$$F(x) = \begin{cases} exp\left\{-\left[1 - k\left(\frac{x-m}{\alpha}\right)\right]^{1/k}\right\} & if\ k \neq 0 \\ exp\left\{-exp\left(-\frac{x-m}{\alpha}\right)\right\} & if\ k = 0\ (Gumbel\ distribution) \end{cases} \tag{1}$$

Where m is a location parameter, α a scale parameter and k a shape parameter. We estimated the parameters using a Bayesian approach. Their posterior density π^* was calculated as

$$\pi^*(m, \alpha, k | \vec{x}) = \frac{l(\vec{\mathbf{x}}|m, \alpha, k)\pi(m,\alpha,k)}{\iiint l(\vec{\mathbf{x}}|m, \alpha, k)\pi(m,\alpha,k)dm\ d\alpha\ dk} \tag{2}$$

Where π is the prior and $l(\vec{x}|m, \alpha, k)$ is the likelihood of the observation vector $\vec{\mathbf{x}}$ given the parameters m, α, k. The denominator makes the integral under the pdf equal one.

We used non-informative priors for the location and scale parameters, (i.e. the location parameter and the log-transformed scale parameter were uniform). A normal distribution with standard deviation 0.2 and expectation 0.0 was used as prior for the shape parameter k, inspired by Coles and Dixon (1999), Martins and Stedinger (2000), and Renard et al. (2013). The likelihood for the systematic data is (see Gaál et al., 2010; Stedinger and Cohn, 1986):

$$l_s = \prod_{i=1}^{n} f(x_i|m, \alpha, k) \tag{3}$$

12

Where $f(x_i)$ is the probability density function for the GEV distribution with the parameter values m, α, k evaluated for the observation x_i. For historical- and paleofloods, it is assumed that all g_j floods that exceed a threshold $x_{0,j}$ for the period j where duration h_j are known. The likelihood of $h_j - g_j$ number of floods not exceeding $x_{0,j}$ during the period h_j is given as:

$$l_{b,j} = \left[F\left(x_{0,j}|m,\alpha,k\right)\right]^{h_j - g_j} \tag{4}$$

Where F is the GEV distribution given in Eq. (1).

We also need to include available knowledge on floods exceeding $x_{0,j}$. In the simplest case we know only that g_j floods exceeded $x_{0,j}$, if so likelihood can be written as:

$$l_{a1,j} = [1 - F(x_0|m,\alpha,k)]^{g_j} \tag{5}$$

Alternatively, we might know that the floods that exceeded x_0 took place within an interval defined by an upper x_U and lower x_L limit:

$$l_{a2,j} = \prod_{o=1}^{g_j}\left[F\left(x_{U,o}|m,\alpha,k\right) - F\left(x_{L,o}|m,\alpha,k\right)\right] \tag{6}$$

And, in optimal scenario, we know the exact magnitude of all floods exceeding $x_{0,j}$:

$$l_{a3,j} = \prod_{o=1}^{g_j} f(y_o|m,\alpha,k) \tag{7}$$

The total likelihood is given as a product of the three major likelihood terms:

$$l_i = l_s \prod_{j=1}^{J} l_{ai,j} l_{b,j} \tag{8}$$

Where J is the number of sub-periods with specific perception thresholds.

The posterior distribution of the parameters was estimated using a MCMC-method implemented in the R-package nsRFA (Viglione, 2012). For estimating return levels, we used the posterior modal values of the parameters. It poses a challenge to set the perception threshold x_0 and length of the historical floods h, i.e. for which period the listed floods represents all floods above the threshold. A simple rule is to set the perception threshold to the lowest observed historical flood value in the historical period. The length of the historical period was decided using the average spacing approach as recommended by Engeland et al. (2018) and Prosdocimi (2018).

3.4.2 Plotting position

The plotting positions provided by Hirsch and Stedinger (1987) that builds on the Cunnane plotting position (Cunnane 1978) were used to plot the empirical distribution of the observations. The exceedance probability p_i of x_i with rank i from a data set with t historical floods representing the historic period h, and s systematic floods with e extraordinary floods is given as:

$$p_i = \frac{i-0.4}{l+0.2} \cdot \frac{l}{n} \qquad i = 1,..,l$$
$$p_i = \frac{l}{n} + \frac{n-l}{n} \cdot \frac{i-l-0.4}{s-e+0.2} \quad i = l+1,...,t+s \tag{9}$$

where i is the rank, l is the number of extraordinary floods ($l = t + e$) and n is the length of the period for which we have information about floods (note that $n = h + s$)

3.4.2 Non-stationary flood frequency modelling

We applied a simple approach to get an estimate of the non-stationary 200-year flood during the recent 1000 year using the paleorecord. In a first step the parameters m', α' and k' in the GEV distribution were estimated using the systematic flood observations. Then we estimated the flood quantiles as:

$$x(F|m',\alpha',k') = \begin{cases} m' + \frac{\alpha'}{k'}\left[1 - \left(1 - ln(F)\right)^{k'}\right] & k' \neq 0 \\ m' - \alpha'\left[ln\left(-ln(F)\right)\right] & k' = 0 \end{cases} \tag{10}$$

Note that by replacing *F* with 1-1/*T* in Eq. (10) we could calculate the flood quantiles for the return period T.

From the sediment core we estimated a time series of the probability of exceedance w_t of the threshold *u*, for each year *t* bycalculating the exceedance rates w_t as the mean number of excesses in a sufficiently large moving window. Further, we assumed that the observed non-stationary exceedance rate influenced both the location and scale parameters with a common factor r_t . From Eq. (10) we found that

$$x(F = 1 - w_t|r_t m', r_t \alpha', k') = r_t x(F = 1 - w_t|m', \alpha', k') = v \tag{11}$$

Since the threshold *v*, and the exceedance rate w_t is known, the factor r_t can be estimated as:

$$r_t = v/x(F = 1 - w_t|m', \alpha', k') \tag{12}$$

The T-years flood for the time t can then be estimated as:

$$q_{Tt} = r_t x(F = 1 - 1/T|m', \alpha', k') \tag{13}$$

4 Results

4.1 Flood variability from the lake sediment cores

The shortest core (FLS113) is 18 cm long, and represent the period 1953-2013 (se Fig. 11). The longest core (FLP213) is 516 cm long and represents the period approximately 0-10 300 years before present (present = 1950) (see Table 5 and Fig. 11)).
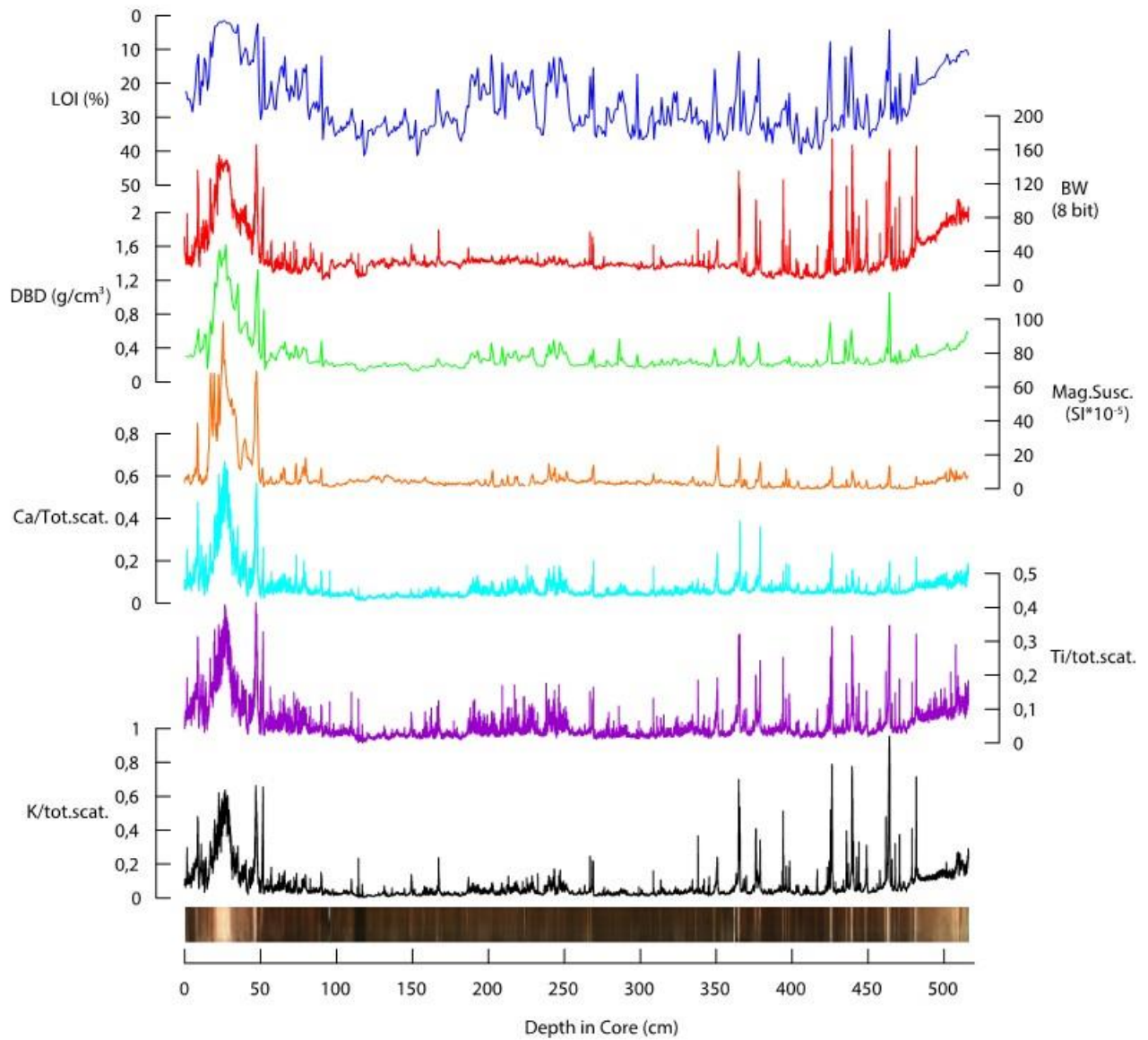
FLP213

The results from the XRF-scan (Ti$_{/total\ scatter}$, Ca$_{/total\ scatter}$ and K$_{/total\ scatter}$) and the greyscale-value (BW) from photo of the core are shown as a function of depth in Fig. 9 together with a photo of FLP213. The core consists of a dark brown gyttja with preserved macro fossils including leaf fragments. This gyttja, carrying a low minerogenic content, is referred to here as 'the background signal' which is characterized by its dark color (BW<30), high LOI (30-40%), low DBD (<0.3 g/cm^3) and magnetic susceptibility (MS) with values close to zero (<5 SI*10^{-5}). Moreover, it returns low K$_{/total\ scatter}$ (<0.03), Ti$_{/total\ scatter}$ (<0.03) and Ca$_{/total\ scatter}$ (<0.03). Interspersed in this 'organic slush' there are narrow (mm scale) light grey (BW 40-170) minerogenic layers with LOI lower than 20%, relatively high density (DBD 0.5-1.0 g/cm^3), higher than average MS with peaks at 15-20 SI*10^{-5} as well as peaks in K$_{/total\ scatter}$ (0.1-0.9), Ti$_{/total\ scatter}$ (0.1-0.4) and Ca$_{/total\ scatter}$ (0.1-0.7). At 33.5-18.0 cm depth in core there is an anomalous thick minerogenic layer with LOI at <2%, DBD at1.6 (g/cm^3), MS at 98 SI*10^{-5}, and very high K$_{/total\ scatter}$ (0.6), Ti$_{/total\ scatter}$ (0.4) and Ca$_{/total\ scatter}$ (0.7).

The correlation matrix (Table 3) shows strong (and significant) correlations between K$_{/total\ scatter}$, Ti$_{/total\ scatter}$, Ca$_{/total\ scatter}$, MS and BW. The weakest correlation is 0.74 between MS and BW which is still very high. LOI is, as expected, negatively correlated with all the other measured variables. We suggest that the main process explaining the relationships between these parameters is driven by the on-off signal related to transport of minerogenic material to Flyginnsjøen during bifurcation events.

1

Figure 9: Results from measured parameters in FLP213. Loss-on-ignition (LOI %) indicated content of organic matter in the core, and are plotted on an inverse scale (blue). BW (red) shows the 8-bit (0-255) black-white values extracted from a photo of the core surface where 0 is black. Dry bulk density (DBD) is plotted in unit gram per cm^3 (green). Magnetic susceptibility (orange) is plotted as $SI*10^{-5}$ as magnetic susceptibility is a dimensionless parameter. XRF-data (K, Ca and Ti) are normalized against total scatter to reduce potential effect of water content.

15

Table 3 Correlation between measured parameters in FLP213 (in bold) and FLS113 (in italic). LoI, BW, DBD, MS and the XRF-data (K, Ca and Ti) were measured in FLP213 whereas CT grayscale, MS and the XRF-data (K, Ca and Ti) were measured in FLP113. LOI (%) indicate content of organic matter in the core, BW is the 8-bit (0-255) black-white values extracted from a photo of the core surface where 0 is black. CT grayscale is a 16-bit number indicate relative densities of the core, DBD is given in unit gram per cm^3 (green). MS is measured as $SI*10^{-5}$ (it is a dimensionless parameter). XRF-data (K, Ca and Ti) are normalized against total scatter to reduce effect of water content. All correlations are significantly different from zero.

	LoI	BW	CT greyscale	DBD	MS	K/total scatter	Ca/total scatter	Ti//total scatter
LoI	1	-0.67 / -	- / -	-0.82 / -	- 0.61 / -	-0.61/-	-0.64 / -	-0.67 /-
BW	-0.67 / -	1	- / -	0.82 / -	0.74 / -	0.89 / -	0.81 / -	0.89 / -
CT greyscale	- / -	- / -	1	- / -	- / *0.79*	- / *0.64*	- / *0.68*	- / *0.59*
DBD	-0.82/ -	0.82 / -	- / -	1	0.86 / -	0.77 /-	0.87 / -	0.82 / -
MS	-0.61 / -	0.74 / -	- / *0.79*	0.86 / -	1	0.76 / *0.66*	0.86 / *0.73*	0.76 / *0.63*
K/total scatter	-0.61 / -	0.89 / -	- / *0.64*	0.77 / -	0.76 / 0.66	1	0.85 / *0.93*	0.96 / *0.95*
Ca/total scatter	-0.64 / -	0.81 / -	- / *0.68*	0.87 / -	0.86 / 0.73	0.85 / 0.93	1	0.91 / *0.88*
Ti//total scatter	-0.67 / -	0.89 / -	- / *0.59*	0.82 / -	0.76 / 0.63	0.96 / *0.95*	0.91 / 0.88	1

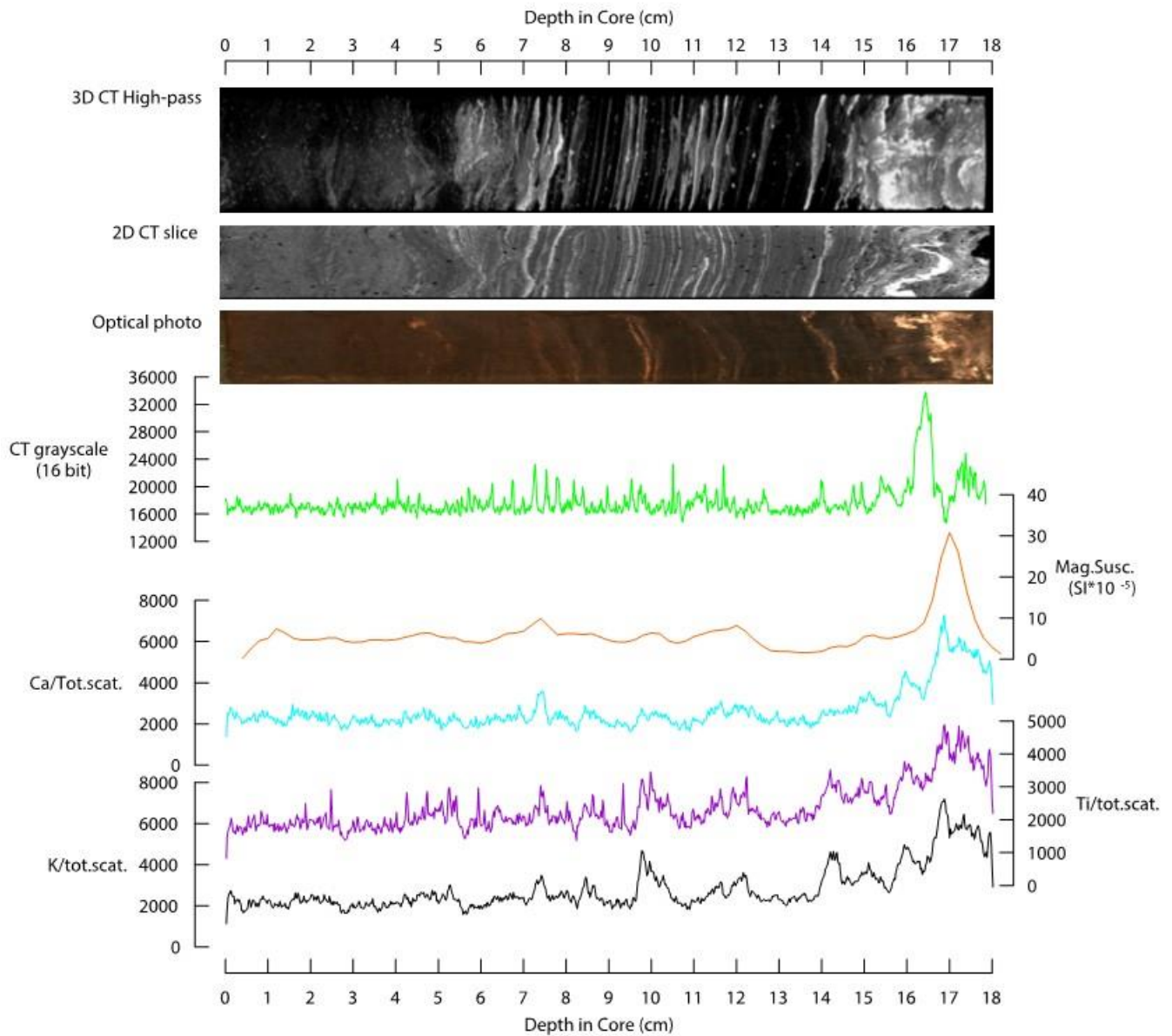## FLS113

This core shows dark organic gyttja with light grey minerogenic layers, similarly to FLS213. The minerogenic layers yield high values of $K_{/total scatter}$ (0.2-0.8), $Ca_{/total scatter}$ (0.1-0.4) and $Ti_{//total scatter}$ (0.1-0.2) as well as slight increase in MS (>6 $SI*10^{-5}$) (Fig. 10). CT data shows that the light grey layers are of high density and reveals numerous thinner layers not visible on photo or in the lower-resolution XRF and MS data. Slight offsets in the positioning of layers in the CT imagery and optical photo occurs due to the fact that the layering is not entirely horizontal.

Correlation coefficients between CT greyscale values, MS, $K_{/total scatter}$, $Ca_{/total scatter}$ and $Ti_{/total scatter}$ in FLS 113 are all over 0.59 and significantly larger than zero. The strongest correlation is seen between $K_{/total scatter}$, $Ca_{/total scatter}$ and $Ti_{/total scatter}$ (Table 3). The somewhat weaker correlation to MS and CT greyscale, and the fact that CT imagery show layering (e.g. 11-12 cm depth in core) not picked up by the other data (Fig. 10), can partly be explained by slight offsets in the positioning of layers between the different scans as well as differences in sampling resolution. The strong correlations and general picture of layered intervals yielding high values, however, indicates that one dominating factor 'controls' the variability, providing further support of the interpretation that transport of minerogenic material to Flyginnsjøen during bifurcation events is the main process.

1

2 Figure 10: Results from high resolution analysis of core FLS113. The top panel shows a 3D CT-visualization of high-density

3 layers (white) in the core. The 2D slice is an 80μm thick slice from the middle of the sediment core. The Optical photo is an

4 RGB photo of the surface of the halved sediment core. CT grayscale plot (green) shows an 80μm grayscale variability along

5 a line through the middle of the sediment core. MS (orange) is plotted as $SI*10^{-5}$ as magnetic susceptibility is a dimensionless

6 parameter. XRF-data (K, Ca and Ti) are normalized against total scatter to reduce effect of water content.

7

8 **4.1.1 Age-depth models**

9 To establish an age-depth relationship for the cores, sediments were subjected to lead dating ^{210}Pb (FLS113) and radiocarbon

10 dating (^{14}C) of FLP213. Measurements were performed by the Environmental Radioactive Research Center at the University

11 of Liverpool (Appleby and Piliposian, 2014) and Poland (Poznan Radiocarbon Laboratory) (Goslar, 2014). The ^{210}Pb and 14C

12 dates used to establish the age-depth models presented in Fig. 11 are listed in Table 4 and 5. Estimation of age as a function

13 of depth for FLS113 was done using a quadratic term regression model of CRS model calculations of the ^{210}Pb with the 1963

14 ^{137}Cs peak at 16.25 cm depth in core (Table 4) as a reference point (Appleby, 2001). For FLP213, we used a Bacon age-depth

15 modelling approach (Blaauw and Christeny, 2011) available in the R-package Bacon. One ^{14}C sample from 51 cm depth in

16 FLP213 was rejected, as this has a stratigraphically reversed age (see Table 5). The age is clearly too old, possibly related to

17

high content of saw dust bringing in relative old carbon core at depth in core. The saw dust may have originated from a saw

mill in the catchment at this time. The 15.5 cm thick anomalous layer at 18.0-33.5 cm depth in core was classified as "slump"

in the Bacon model, and thus interpreted as an instantaneous event deposit. This layer has a basal age estimate of 1776 CE

from the age-model, and is likely to be related to the historically documented 1789 CE Stor-Ofsen flood event (see Sect. 3.2).

Table 4: Fallout radionuclide concentrations and chronology for FLS113 from Flyginnsjøen.

Depth (cm)	$^{210}Pb_{Total}$ (Bq kg^{-1})	±	$^{210}Pb_{Unsupp.}$ (Bq kg^{-1})	±	$^{210}Pb_{Supp.}$ (Bq kg^{-1})	±	^{137}Cs (Bq kg^{-1})	±	Year	Uncertainty (years)
0									2013	1
0.25	809.5	47.9	702.3	49.2	107.2	11.3	65.7	7.2	2013	1
1.25	686.2	33.4	585.9	34.0	100.3	6.6	63.3	5.3	2011	1
2.25	570.9	21.6	492.4	21.9	78.5	3.9	62.0	3.4	2009	1
3.25	598.8	22.6	524.3	23.0	74.5	4.2	72.7	3.7	2007	2
4.25	549.2	21.5	474.9	21.9	74.2	3.9	82.9	4.3	2004	2
5.25	455.9	17.5	386.0	17.8	69.8	3.1	77.6	3.4	2000	2
6.25	482.0	25.2	404.0	25.6	78.0	4.7	64.0	3.9	1998	2
8.25	515.6	20.4	442.3	20.7	73.2	3.7	58.9	3.3	1992	3
10.25	391.4	19.3	329.6	19.6	61.8	3.6	84.6	3.7	1986	3
12.25	331.6	15.3	266.2	15.6	65.4	3.0	78.1	3.1	1979	4
14.25	231.2	12.8	173.4	13.1	57.9	2.6	68.0	2.8	1970	5
16.25	226.4	13.8	152.8	14.1	73.7	3.1	138.8	4.1	1962	6
17.25	193.3	13.3	140.7	13.5	52.6	2.7	50.7	2.4	1957	6
19.25	112.9	7.3	68.8	7.4	44.1	1.6	9.2	1.2	1948	7

Table 5: ^{14}C-dates for FLP213 from Flyginnsjøen. Radiocarbon ages are calibrated using the IntCal 13 calibration curve

(Reimer et al., 2013)

Lab. Nr.	Depth in core (cm)	^{14}C age. yr BP	Cal. yr BP (most prob. 68.3% conf int.)
Poz-57974	51	870 ± 30	732 –796 (0.97)
Poz-59030	70	390± 30	453 – 503 (0.78)
Poz-57975	118	1565± 35	1455 – 1521 (0.73)
Poz-57976	206	2860± 40	2924 – 3037 (0.91)
Poz-57977	304	4125± 40	4571 – 4653 (0.49)
Poz-57978	370	5670± 40	6409 – 6487 (1.00)
Poz-59029	401	6535± 35	7424 – 7476 (1.00)
Poz-57979	462	8180± 50	9028 – 9140 (0.75)
Poz-57980	504	9190± 50	10259 – 10403 (1.00)
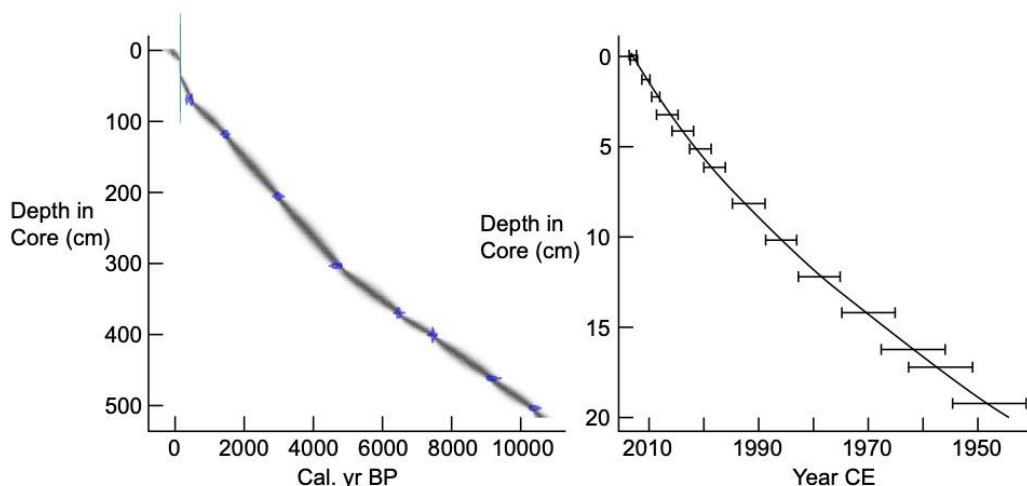
Figure 11 Age-depth model for FLP213 (right) and FLS113 (left). Note the step in the FLP213 age-depth model at 33.5 – 18.0

cm depth in core related to the *Stor-Ofsen* flood event in 1789 CE.

4.1.3 Identification of flood layers in FLS113.

We used the concentration of $Ti_{/total\ scatter}$ and $K_{/total\ scatter}$ from the XRF-scan of FLS113 to establish a link between dense, minerogenic sediment layers and the 22 bifurcation events between 1953 and 2013. Note that XRF data ($K_{/total\ scatter}$, $Ca_{/total\ scatter}$ and $Ti_{/total\ scatter}$) correlates strongly with the CT-scan (greyscale values), and MS for both FLS113 and FLP213 (Table 3), and this suggests the flood transported material originate from a one source and that this is constant over time. All detected layers are thus interpreted to be related to the same process bringing minerogenic material to Flyginnsjøen. The first step in our approach was to transform the depth of the XRF-scan to age using the depth-age model for FLS113. After having identified the flood layers, we used the algorithm described in Sect. 3.3.1 to identify local peaks in the measured parameter. We used a time window of 1 year, a value of 680 and 527 for $Ti_{/total\ scatter}$ and $K_{/total\ scatter}$ respectively for h_1 and $h_2 = 0.5 * h_1$ which identified 23 local peaks for $Ti_{/total\ scatter}$ and $K_{/total\ scatter}$ over the same period that we observe 22 bifurcation events. A time series of the bifurcation volumes and the XRF-scan data can be viewed in Fig. 12. Taking into account the uncertainty in the dating (Fig. 11), we see that five of the bifurcation events do not correspond directly to a sediment layer. All the three largest flood events were, however, correctly identified, and considering the uncertainties in the age-depth model this supports our working hypothesis that sediment layers can be used to identify flood events caused by episodes of bifurcation at Kongsvinger.
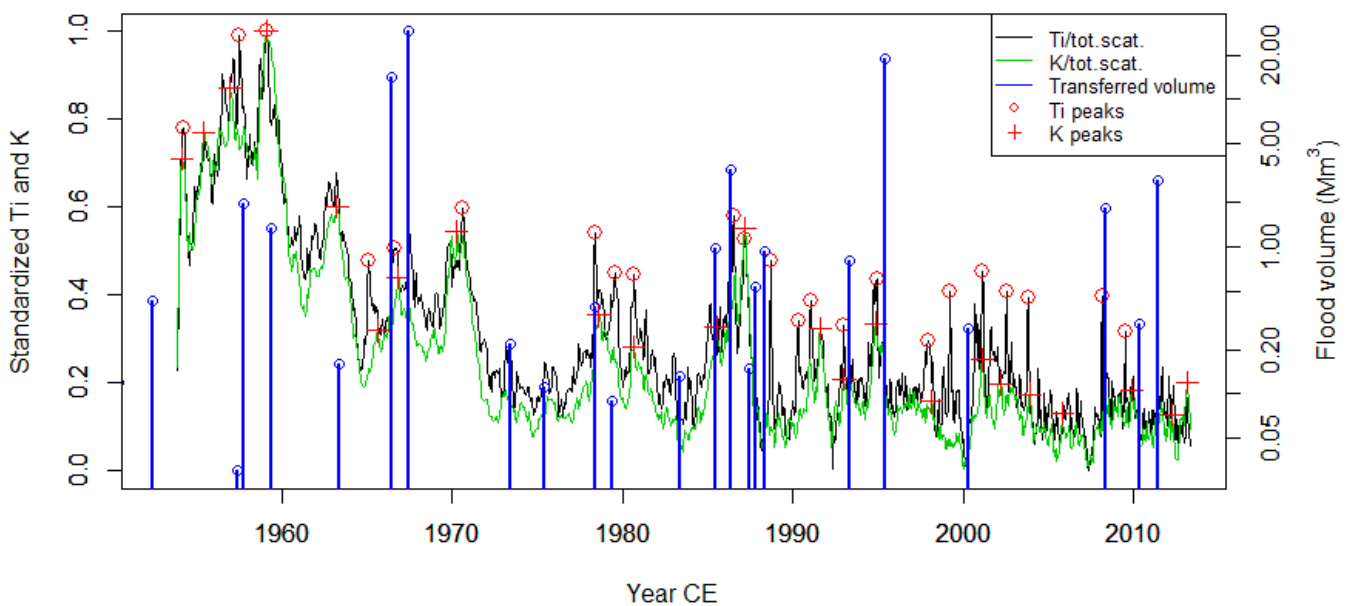

Figure 12. Transferred volume of the 23 bifurcation events in the period 1950-2013 CE (in blue) and the 24 identified flood-layers (red) identified using XRF scans of $Ti_{/total\ scatter}$ and $K_{/total\ scatter}$ for FLS113.

4.1.3 Frequency of flood events during the Holocene.

From FLS113 we have established a link between dense, minerogenic sediment layers and bifurcation events. We therefore assumed that the analyses of FLP213 could be used to produce a time series of flood events covering the last 10 300 years. Here we used the local peak detection algorithm presented above to identify sediment layers with high concentration of $K_{/total\ scatter}$ and $Ti_{/total\ scatter}$. Since the uncertainty range in the age estimate is 30 to 50 years, we calculate the average rate of a given flood event within a moving Gaussian time windows of 50 years for both $Ti_{/total\ scatter}$ and $K_{/total\ scatter}$ (Fig. 13). The standard

1 deviation of the estimated flood rate $\hat{\lambda}$ was calculated as $\hat{\lambda} \pm z\sqrt{\frac{\hat{\lambda}(1-\hat{\lambda})}{50}}$ and it was used to assess the 95% confidence intervals.

2 We see that the flood counts using $Ti_{/total\ scatter}$, $K_{/total\ scatter}$ and BW to a large degree overlap and follow the same Holocene

3 trends, as anticipated due to the high correlation coefficient between the two (see above).
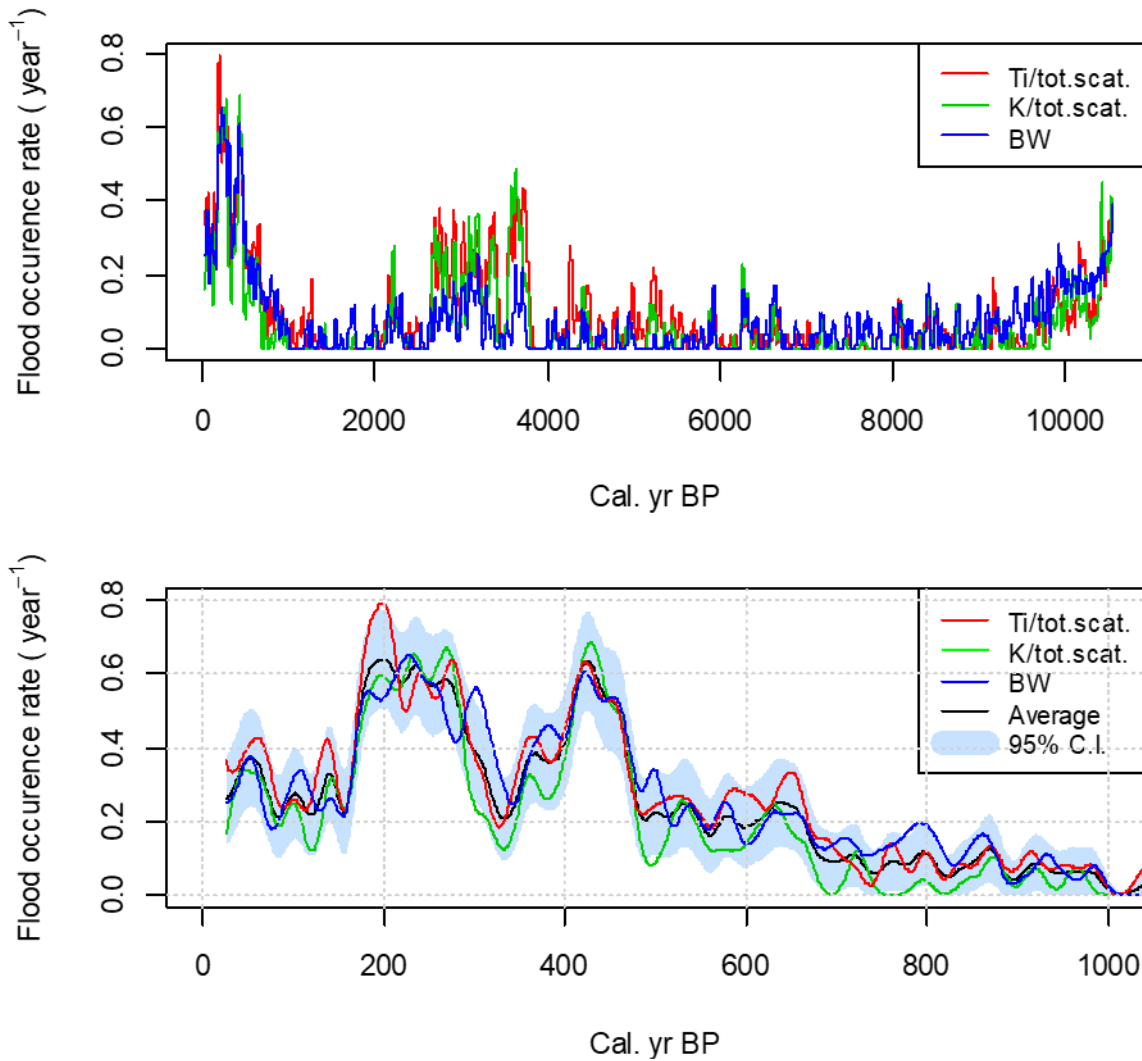
4

5 Figure 13: In the top panel, average flood rate per year calculated in a 50-years moving window during the Holocene. In the

6 lower panel, the recent 1000 years are shown only. The lower panel also include a 95% confidence interval for the average

7 flood rates. The flood rates were identified by detecting local peaks in $Ti_{/total\ scatter}$, $K_{/total\ scatter}$ and BW values.

8

9 **4.2 Stationarity of flood frequency in the paleo-flood data**

10 A key observation in the Holocene flood frequency reconstruction is the large non-stationarity played out across multiple time

11 scales. We observe that there are two major flood rich periods during the Holocene (Fig. 13, upper panel). The first runs from

12 3800 to 2000 cal. yr BP when it ends abruptly. The second period extend from around 700 cal. yr BP up to present day. Looking

13 at flood frequency over the recent 1000 years (Fig. 13, lower panel) we observe significant internal variability within the flood

14 rich period. The period with the highest flood rates occurs in the 18th century, but also in the 15th century.. The data from

15 FLP213 informs us that the flood event in 1789 is truly an anomaly, as is evident from the sheer amount of sediments deposited

16 during this event (no other flood comes close), and it also yield the highest measured values of e.g. density (DBD) as well as

17 magnetic susceptibility (MS) throughout the core (Fig. 9). It is therefore reasonable to assume that the 1789 CE flood was an

18 extraordinary event making it the largest during the entire time span of the record, i.e. 10 300 years.

20

4.3 Flood quantile estimation by combining systematic-, historical- and paleo-flood data

The flood quantiles combining the systematic, historical and paleodata have been analysed in different, but complementary ways. Table 6 provides an overview of the flood information related to data source and the time intervals they represent. The first step was to estimate the flood quantiles using only systematic data. In the second approach we added all the historical flood data. The smallest historical flood of 2533 m³/s was used as the threshold x_0. The length of the historical data period was calculated based on Prosdocimi (2018) and Engeland et al. (2018).. Since the average waiting time between the historical floods is 22 years, the start of the historical period was set to be 22 years before CE 1675 (i.e. the year of the oldest historical flood) The historical period ended in CE 1871 giving $h = 219$ years. The exact sizes of the historical floods (Table 1) was assumed. In the third approach we used the paleo-record as a guidance to weigh the historical information. Since paleorecord indicates that the historical floods in the 18th century occurred in a flood rich period, we used only the historical flood events from the 19th century. Moreover, the historical flood from CE 1789 was included, and it was suggested that this was the largest flood during the last 10 000 years for reasons explained above. The results are shown in Fig. 14, and we see that the results are sensitive to the assumption of which period the CE 1789 flood represents.

Table 6 Overview over the three data sources used for flood frequency analysis.

| Data source	Period	# floods	Threshold (m³/s)
Systematic flood data	1872-1936	-	-
Historical flood data	1653-1871	9	2533
Paleo Flood data	1300-1871	208	1800
Paleo Flood data when combined with historical flood data	1300-1651	110	1800
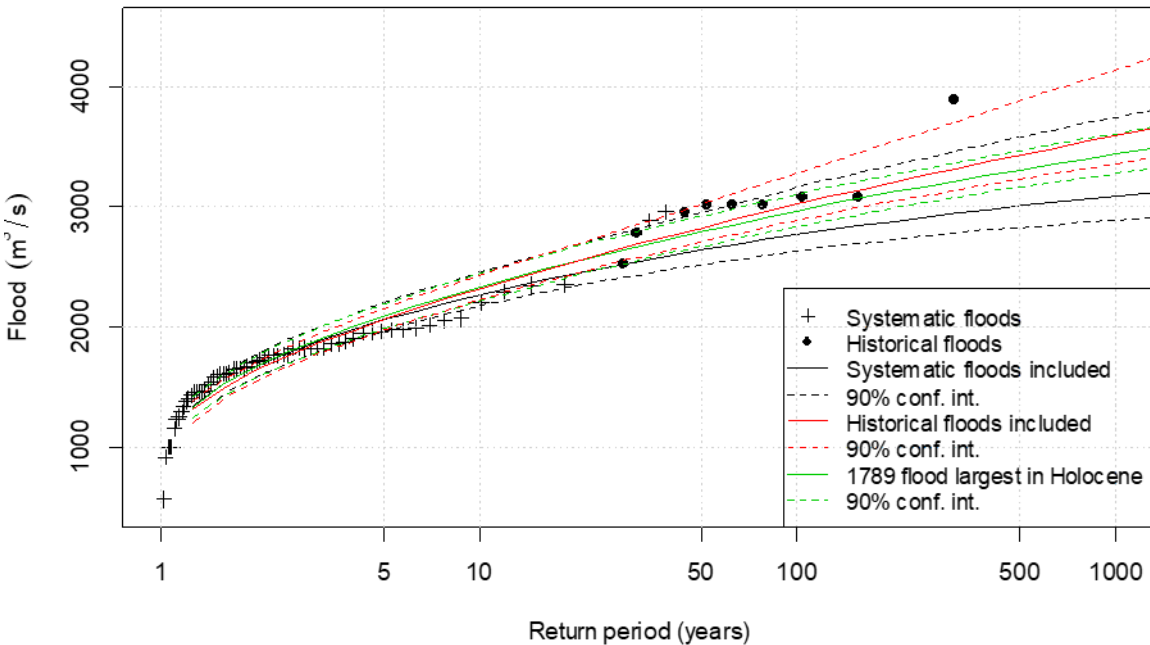
Figure 14: The sensitivity of flood frequency analysis to three different combinations of systematic and historical flood data. Annual maximum floods for the period 1872-1836 were used as systematic flood data. Nine historical floods exceeding 2533 m³/s and representing the period 1653-1871 were used as historical floods. Based on the paleorecord, the CE 1789 flood was

1 reweighted to represent a period of 10 000 years. The plotting positions for the systematic and historical floods are based on

2 Hirsch and Stedinger (1987) and explained in Section 3.4.2.

3

4 The next step was to include the paleo-flood information in the flood frequency analysis. We did this in two ways: (i) we

5 combined the systematic data and the paleodata and (ii) we combined systematic, historical and paleodata. For the paleodata

6 we used 1800 m^3/s as the threshold x_0 since it provided the same number of flood events (i.e. 19 events) from the paleo record

7 and the streamflow observations for the overlapping time period (1891-1950). When we combined the systematic data and the

8 paleodata we counted 208 flood events representing a period of 572 years (1300-1871 CE) When we combined the systematic,

9 historical and paleodata, we counted 110 events for a period of 353 years (1300-1652 CE) from the paleodata and used the 9

10 historical floods representing the period1653-1871. The results are shown in Fig. 15. We see that the estimates are sensitive to

11 historical information. The paleodata did not impact the result to the same degree.
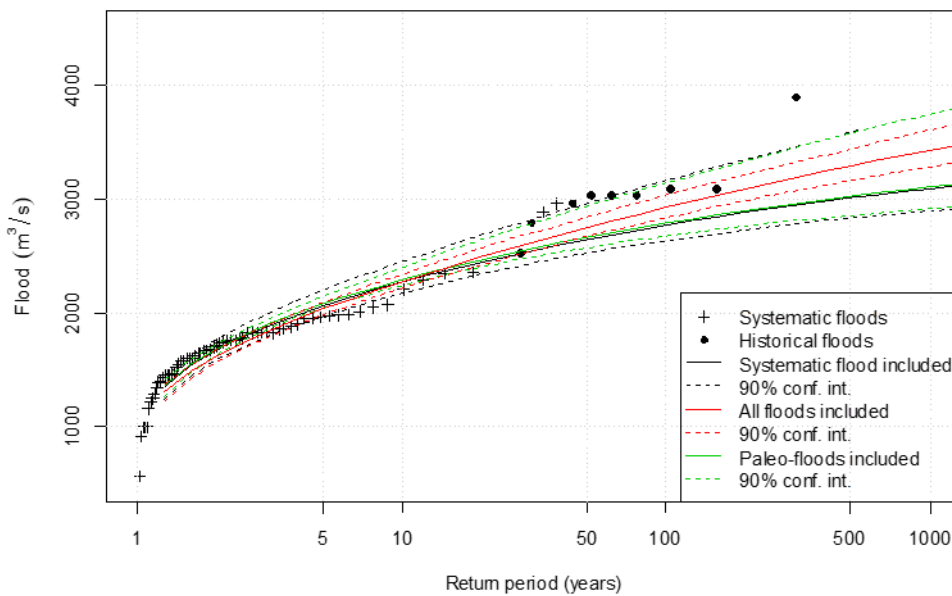
12

13 Figure 15. The sensitivity of flood frequency analysis to three different combinations of systematic, paleo, and historical flood

14 data. Annual maximum floods for the period 1872-1836 were used as systematic flood data. Paleo-foods representing 208

15 events exceeding 1800 m3/s for the period 1300-1871. When all flood data were combined, the paleo-floods represent 110

16 events for the period 1300-1652, and nine historical floods exceeding 2533 m3/s and representing the period 1653-1871 were

17 used as historical floods. . The plotting positions for the systematic and historical floods are based on Hirsch and Stedinger

18 (1987) and explained in Section 3.4.2.

19

20 To achieve a nonstationary estimate of the design flood, we used the flood occurrence rate presented in Fig. 13 to estimate the

21 200-years flood in a moving time window as explained in Sect. 3.4.2. We used 1900 m^3/s as the threshold v in Eq. (11) since

22 it provided a good agreement between the 200-years flood estimated from the systematic data and the non-stationary 200-years

23 flood for the overlapping period. The results are presented in Fig. 16. We now see that the size of the 200-years flood is non-

24 stationary. During the 'Little Ice Age' (LIA) it was up to 23% higher than in present climate, whereas during the period 4000-

25 6000 B.P it was around 30% lower than today.
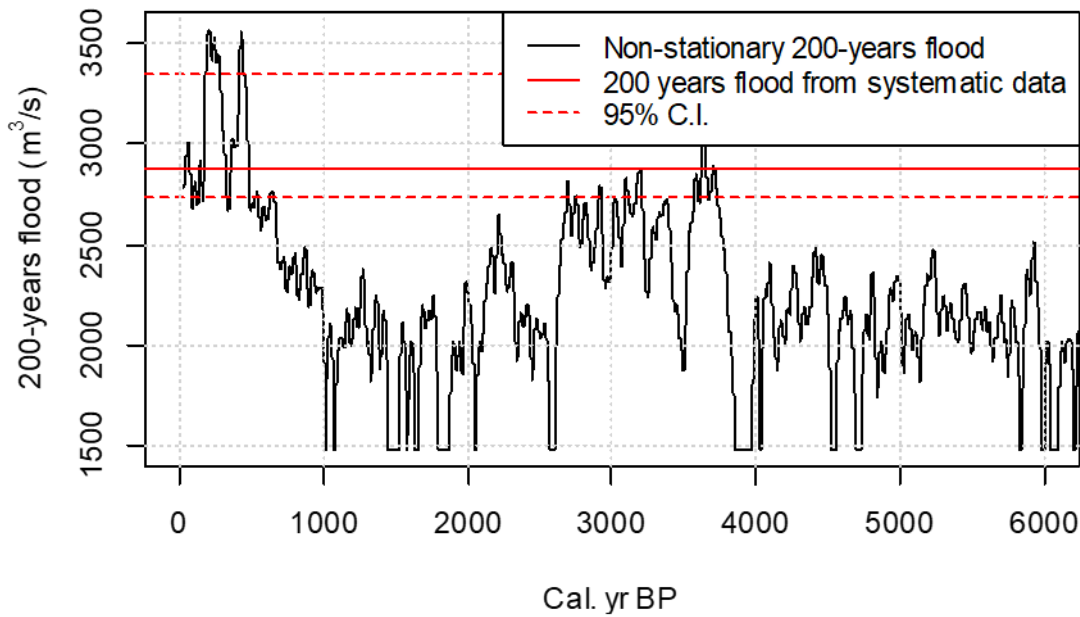
Figure 16: Non-stationary estimate of the 200-years flood for the resent 6000 years. The red lines indicate the estimated 200-years flood and the 95% confidence intervals estimated using systematic streamflow observations.

5.0 Discussion

5.1 The reliability of the historical data and the paleoflood records

The historical data applied in this study are marked as water levels at the flood stone at Elverum, and the associated flood discharges are estimated by Hegge (1969). An assumption for these estimates is that the river profile is relatively stable over the historical period, and in particular that the large flood in CE 1789 did not cause any substantial changes. This is a reasonable assumption because, although four large floods occurred between CE 1781 – 1969, only one rating curve is used for the period. The gauging station was moved around 660 meters in 1969.

During the last decade or so lakes across Europe have been studied in detail and high-resolution paleoflood records have been produced from both the low-lands and the high-lands (Cf. Wilhelm et al., 2018). Unlike many of these studies, we have worked with lakes that *only* receive flood-delivered sediments whenever the local river (Glomma) exceeds a certain well-known threshold (1500 m^3/s). This setting tends to suggest that not only are we working with a sedimentary archive that filters out noise, but also one that provides a minimum estimate of the discharge associated with the floods recorded. The flood information extracted from the lake sediment cores, nevertheless, relies on a set of assumptions that is discussed in the following.

The first assumption is that all flood events recorded in lake Flyginnsjøen are directly related to Glomma. Linking the sedimentary signal in FLS113 to specific individual flood events in Fig. 12 is challenging. Due to the uncertainties in the age-depth model we have not found a good way to estimate probabilities for correspondence. Consequently, we rest on the assumption that our 23 recognized peaks in the sedimentary signal corresponds to the 24 bifurcation events over the same period based on the visual correspondence between peaks in K and Ti and flood volumes shown in Fig 12. We cannot completely rule out the possibility that minor floods in the local catchment of Flyginnsjøen occurred simultaneously with floods originating from Glomma or even just within the very small catchment surrounding the lake due to local rainstorm events. Given the heavy vegetation cover in the catchment of Flyginnsjøen, its small size and the low-angles of the slopes leading into the lake, we deem the possibility of a local sedimentary imprint as very low. This is supported by both XRF and

MS data. A thorough sedimentary analysis of potential sediment sources in the Glomma catchment could add valuable information to the composition of the recorded flood deposits, and perhaps even denote source areas and thus also flood triggering mechanisms of individual flood events (cf. Støren et al 2016). The 154450 km2 size of the Glomma catchment, and the mixing process involved, would however require a very large number of comparative samples. Moreover, he consistency in bifurcation events causing peaks in concentration in both $Ti_{/total\ scatter}$ and $K_{/total\ scatter}$, as well as MS, suggests that the source region for this signal remains the same throughout the record. The most likely source is thus the abundant glaciofluvial material available in the area between Tarven and Flyginnsjøen (see Fig. 4).

A second assumption is that the river channel and landscape geometry controlling the bifurcation events has not changed over the approximately recent 10 000 years to the extent that it alters this interplay between a flooding Glomma and the investigated lake. The current river geometry was shaped by a glacial lake outburst flood (GLOF) some 10 000 - 10 400 years ago with a peak discharge of more than 10^6 m^3/s (Høgaas and Longva, 2016). This GLOF flushed the valley where Glomma runs and also established the current river channel at Kongsvinger (Pettersson, 2000). Based on Klæboe (1946) and Hegge (1968), the threshold between Vingersjøen and Flyginnsjøen (Fig. 4) is a resilient and stable topographic feature. The intermittent drainage patterns that route water from Vingersjøen to Flyginnsjøen during the bifurcation events may have undergone some changes during the course of time, but it's hard to see how this would directly influence the deposition of flood-delivered sediments to Flyginnsjøen. According to Hegge (1968), the flood events that occurred in 1967 CE and 1968 CE caused some erosion at the very highest elevation of this intermittent water course. Having said that, these flood events did not cause any major damages to this area (Klæboe, 1946). In recent years, denser vegetation and also the construction of a road bridge has potentially lessened the transfer capacity between the lakes although we have little or no evidence for this based on what we observe in the lake core.

The resolution of the XRF signal is on average sub-annually, but because the uncertainty in the age-depth we calculated flood rates, i.e. average number of flood events, for a moving 50 years window. Unlike the findings of Evin et al., (2019), and although the floods are of varying magnitude, there appears to be no systematic relationship between flood sizes and sediment thickness or volume except for the *Stor-Ofsen event*. This is probably explained by the fact that the sediment transport for individual floods will in part be deposited in the two preceding lakes (Vingersjøen and Tarven) buffering Flyginnsjøen (Fig. 4), but may also indicate that event-specific features such as ground frost or snow cover may regulate sediment availability.

5.2 Non-stationarity in flood records and regional climate co-variability

The paleoflood data presented here document that the flood frequency is non-stationary during the last 10 300 years being manifested on multiple time scales (Fig. 13). Non-stationarity is typically identified as quasi cyclic flood-rich and flood-poor periods (for European studies, see e.g. Brázdil et al., 2005; Glaser et al., 2010; Hall et al., 2014; Jacobeit et al., 2003; Kundzewicz and International Association of Hydrological Sciences., 2012; Mudelsee et al., 2004; Swierczynski et al., 2013) where the flood rich period may last for 50-60 years (e.g. Glaser et al., 2010). Over the instrumental and the historical era, floods in the Glomma catchment have mainly occurred in late spring (late May, early June) due to the sudden melting of large snow reservoirs following a steep rise in temperatures that often overlaps with persistent rain (Roald, 2013). Under the current climate conditions, the largest floods in the Glomma catchment are caused by (i) high winter precipitation and preferentially cold winters resulting in a large snow storage (ii) a cold spring followed by a sudden increase in air temperature producing high melt rates and (iii) large amounts of widespread precipitation combined with snow melt (Vormoor et al., 2016). Importantly, for these spring-snowmelt triggered floods, the soils are either frozen and/or already saturated with moisture channeling shallow sub-surface flow and overland flow resulting in a fast discharge response to snowmelt and rain. Based on these observations, we hypothesize that on decadal to centennial time scales, increasing flood sizes can be explained by

increasing precipitation, in particular during winter and spring, and cool winter temperatures. Increasing spring and summer temperatures might potentially lead to increasing flood sizes, but this effect depends strongly on the snow storage available for melt.

In Figure 17 and 18 we compare the flood frequency reconstruction from Flyginnsjøen to several climate reconstruction representing temperature and precipitation on a centennial to decadal scale variability. In Figure 17, the flood frequency is compared to regional summer temperature reconstructions (Moberg et al, 2005), whereas it is compared to local records of glacier variability (upper panel), a flood index (second panel) and local July temperature (third panel) in Figure 18. No continuous reconstructions of winter precipitation are available for this region, however, the glacier growth in Scandinavia is primarily driven by summer temperatures and winter precipitation, and the reconstructed flood record is therefore compared to glacier variability in Rondane in the upper Glomma catchment. Low values of the flood index produced by Støren et al (2012) reflects periods with relatively high flood frequency in eastern Norway. We observe co-variability between the reconstructed flood frequency in Flyginnsjøen and several of the climate reconstructions which may indicate that the non-stationarity of flood frequency is, to a large degree, related to non-stationarities in climate. The data from Flyginnsjøen shows, for instance, two distinct intervals with high flood frequency during the 'Little Ice Age' (LIA), both played out on centennial time scales. During this period the average summer temperature for the northern hemisphere did not change substantially. The dip in flood frequency around year 400 BP might be explained by other climate variables like winter precipitation. Since 1850 there's been a steady increase in summer temperature followed by a reduction in flood frequency. Enhanced flooding during the LIA is observed in other lake studies from eastern Norway as well, including Atnasjø (Nesje et al., 2001), Butjønna (Bøe et al., 2006), Meringdalsvannet (Støren et al., 2010) and also the river Grimsa in the headwater of Glomma (Killingland, 2009).
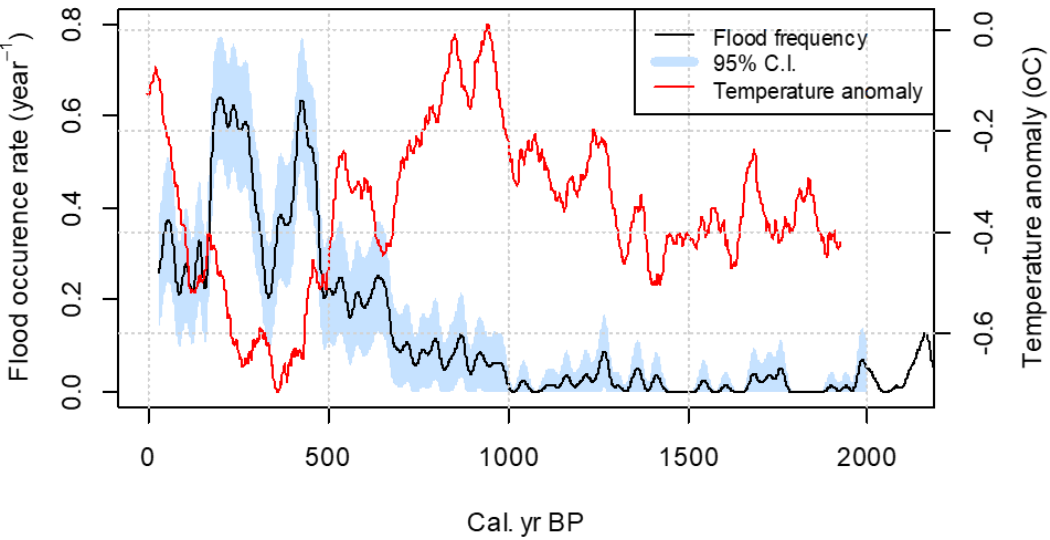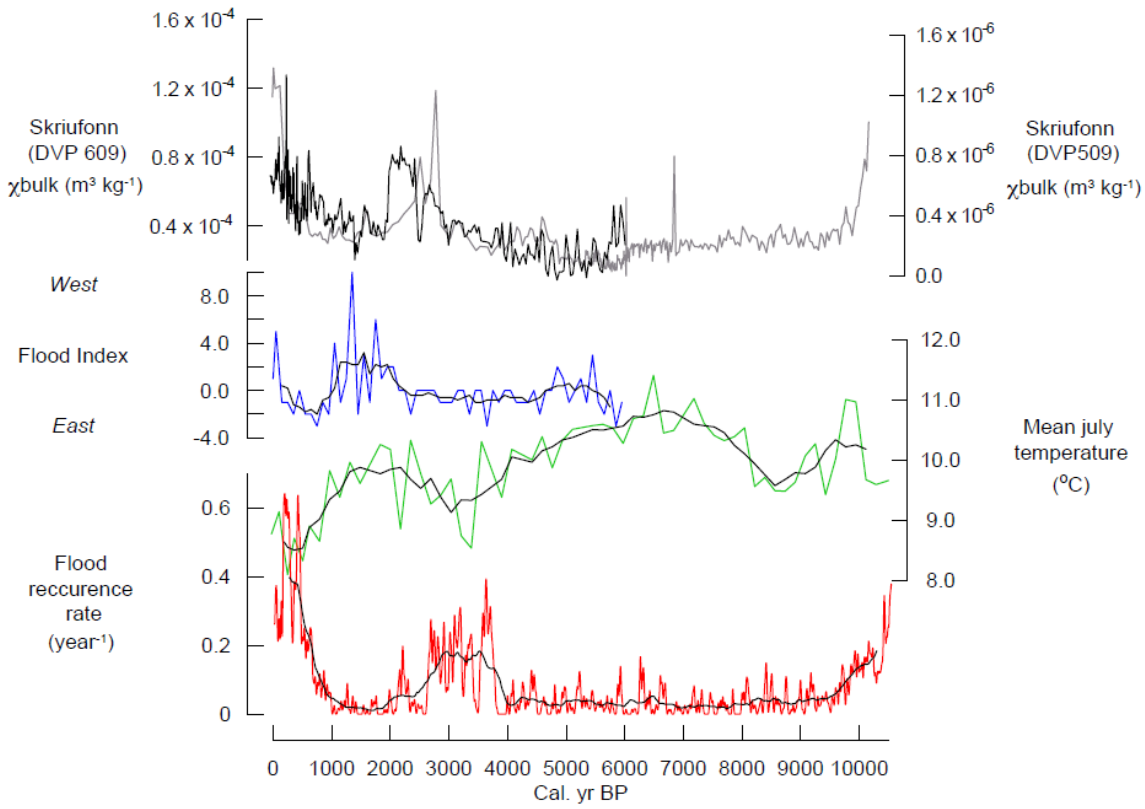

Figure 17: Flood frequency in Glomma (blue bars) and 30 years moving average Northern Hemisphere summer temperature anomaly from Moberg et al. (2005).

Another period with heightened flood activity occurs roughly between 4000 to 2000 years ago. The increase in flood frequency in Glomma during this period, and also during the LIA interval, coincides with a recorded decrease in summer temperature at Bruskardstjørni in eastern Jotunheimen (Velle et al., 2010) and increasing glacier growth in Rondane (Kvisvik et al., 2015), the mountainous source area of Glomma (Fig. 18). Multi-decadal periods are typical superimposed on centennial trends, as is the case for both these two flood rich intervals. The near absence of floods prior to 4000 years ago is another recurring feature in all flood records from Eastern Norway (e.g., Støren et al., 2016). Locally, it seems plausible that the effect of raising the 0-

1   isotherm with 100-300 m altitude, the effect of a warmer summer season, will significantly change the potential storage of
2   snow (Støren & Paasche, 2014).

3   The observed changes in flood frequency occurring both during the LIA and in the first half of what sometimes is
4   called the Neoglacial era (4000-2000 years ago) can thus, at least partially, be explained by the combined effect of the flood
5   generating processes (cf. Vormoor et al., 2016). The near-absence of floods prior to the onset of the Neoglacial, when summer
6   temperatures were ca 1°C higher than today (Velle et al., 2010), may be a valuable albeit imperfect analogue for the coming
7   century. During this period the 200-years flood is around 30% lower than today (Fig. 16).
8   In large catchments where snow melt is the primary flood generating process, it is suggested that we will may see smaller
9   flood sizes for easter Norway according to Lawrence (2020). For small catchment, in western Norway, where rain-generated
10 floods already dominate, floods are expected to increase. Cooler temperatures, especially in summer and spring are likely to
11 delay the melting of the snow-cover – a scenario increasing the probability for a sudden warming simply because it occurs
12 later in the season.

13
14 Figure 18: Flood frequency in Glomma (red) with 500yr running average, --reconstructed summer temperature from
15 Brurskardtjørni, southern Norway (Velle et al., 2010) (green) with 5-point running average, Flood index (blue) with 5-point
16 running average (Støren et al., 2012) showing relative distribution of flood recurrence rate over southern Norway. Glacier
17 activity at Skriufonn, Rondane southern Norway (Kvisvik et al., 2015) (Black and purple)

18

19   The increase in flood frequency commencing at c. 4000 yr BP is a reoccurring feature not only in Europe but also in
20 parts of the USA (Paasche and Støren, 2014). This hints at a large-scale change in the climate system at the time, with
21 implications for both atmospheric circulation patterns and temperature trends. This major climate shift recorded in Europe is
22 noteworthy because the flood seasonality is different across such a large area for many reasons, including the varying altitudinal
23 differences. In high-lying areas in Austria (north of the Alps, Swierczynski et al., 2013), and in the and in the Central Alps
24 (Switzerland and northern Italy, Wirth et al., 2013) floods start to increase, as in eastern Norway, rapidly just after 4000 years
25 ago and remain on average high until 2000 years ago. Studying the relative distribution of floods in Norway, Støren et al.
26 (2012) suggest that the long-term trends in the floods is dependent on changes in the distribution of winter precipitation related

26

to semi-permanent shifts in atmospheric circulation patterns, and that an anomalous strong meridional component in the atmospheric circulation pattern are linked to floods in eastern Norway. Over the time period between the two flood rich periods in Glomma (c. 2000-1000 yr BP), Støren et al. (2012) recorded a westward shift in the flood frequency likely caused by reduced precipitation in the eastern areas (Fig. 18).

There are also potential catchment feedback mechanisms, not necessarily related to climate, that can both dampen and boost the flood patterns. Humans can potentially influence the landscape by forest clearing which would alter sediment availability and run-off patterns as well as change the overall buffering capacity.

The flood-rich period occurring between 2500-4000 yr BP coincidence largely with the bronze age (2500-3700 BP) when settlements and farming expanded in Norway (REF?), but whether this early colonization impacted flood patterns remains an open question. Its worthwhile noticing that this interval with increased flooding is also recorded in other lake sediment records from Southern Norway (Støren et al., 2010; Bøe et al., 2006) which was only marginally impacted by human activity if at all (shown in Fig. 18) by farming. We therefore argue that the effect of land-use cannot be the main explanation for the observed changes in flood frequency during this period. A similar conclusion was reached by Shubert et al., (2020), who show that logging and agricultural activities around lake Mondsee, Austria, was low during flood rich periods, and that the flood record reflects climate variability rather than human activity in the catchment.

In more recent times, deforestation is a candidate that potentially could help explain the increase in flood frequency after 1600 CE. The mining industry that started in Norway in the late 16th century required a large amount of timber which resulted in widespread deforestation in Glomma's upper catchment. This removal of woodland cover may have influenced the local erosion and sediment transport of the upstream Glomma catchment, but because this is area represents only a fraction of the total catchment area, we think that these 'excess sediments' would be diluted downstream. Another relevant point here is that the flat downstream gradient of the river Glomma, potentially causing sediment deposition long before they reach the bifurcation point at Kongsvinger. A final point is that the sediment source for the flood layers deposited in Flyginnsjøen is suggested to be mainly local, and the area around the lake and the location for the bifurcation events itself was not subject to removal of woodland in this period. It is possible that the removal of woodland amplified the size (and frequency) of floods since forests, in most cases, reduces flood peaks. This, however, require a more regional and systematic vegetation change than that related to mining in the upper Glomma catchment to affect the 154450 km^2 large catchment. Some of these mechanisms discussed above could potential help explain why *Stor-Ofsen* in 1789 is the largest local flood on record. As mentioned, this flood deposited the thickest sediment layer in the entire record from Flyginnsjøen. The anomalous sediment thickness is also recorded in lake sediment archives for other places in eastern Norway (see Bøe et al., 2006). Another amplifying process that can make floods become larger, and also remobilizing lager amount of sediments, as is the case for *Stor-Ofsen*, was the large number of upstream landslides that took place at the time (Roald, 2013). In fact, the summer of 1789 was named 'skriusommaren' (the landslide summer) in historical material (Roald, 2013).

5.3 Flood quantile estimation by combining systematic-, historical- and paleoflood data

The non-stationarity in flood frequency is a major challenge when estimating flood quantiles used for land planning and design of infrastructure given that one needs to predict how the flood frequency will evolve over the life time of the construction, e.g. for bridges it is 100 years (Koh et al., 2014). Milly et al. (2008) argued that 'stationarity is dead' and that it is necessary to account for non-stationarity in order to avoid under-estimation of risks based on design floods.

Conversely, Serinaldi and Kilsby (2015) posited that 'stationarity is undead' because a stationary model is robust and can be a useful reference/benchmark. Accounting for uncertainty in a stationary model can be as important as including non-stationarity within a risk assessment framework. A non-stationary model introduces more parameters and thereby, in most

cases, increases the estimation uncertainty. An additional challenge when applying a non-stationary model for design flood estimation is to project the flood frequency into the future.

The paleoflood data presented here suggests that the flood frequency is non-stationary and that there is indeed flood rich and flood poor periods (Fig. 13). Since design flood estimates are used for assessing average risk over the lifetime of a construction, it is desired that design flood estimates are stable over time and not sensitive to quasi cyclic variations in flood sizes on annual to decadal time scales. It is, however, important to account for trends or shifts in flood frequency. Macdonald et al. (2014) show that on centennial time scales, the effect of cyclic variations in short systematic records can effectively be removed by a temporal extension of flood time series using historical information. Data from Flyginnsjøen and historical data reveals that a quasi-stationary period can be identified at centennial time scales, but not on a sub-millennium time scale where major shifts in flood frequency are identified (Fig. 13).

In this study, we firstly used the stationarity assumption and evaluated several possible ways to combine the three data sources within a stationary framework. The results in Fig. 14 and 15 show that the design flood estimates are sensitive to how we combine the systematic, historical and paleo flood data. We used 65 years of systematic data covering the period CE 1872 – 1936 for which we assume that the effect of river regulation is negligible. Adding the historical data from the flood stone covering the period from CE 1653 to 1871, substantially increased the estimates of the flood quantiles and slightly reduced the estimation uncertainty (Fig. 14).

The paleoflood timeseries provided here suggests that the flood frequency during the historical period is non-stationary where the 18th century was an extremely flood rich period (Fig. 13), and that the CE 1789 flood was an exceptional flood during the 10 300 years covered by the sediment core. Based on this paleo-information, we used historical data from the 19th century, and added the CE 1789 flood by assuming it was the largest flood over a period of 10 300 years. This slightly reduced the flood quantile estimates as compared to using all historical information and substantially reduced the estimation uncertainty (Fig. 14). These results show that for the site at Elverum, we should be careful when including historical flood information from the flood rich period in the 18th century.

As a next step, we added the paleo-flood data representing 572 years (i.e. CE 1300-1871). This resulted in negligible differences in flood quantile and uncertainty estimates (Fig. 15) indicating that the information content in the paleodata alone can be small. A possible explanation is the combination of the relatively low threshold (according to Fig. 15 it is around a 5-years flood), and that we only had information about the number of flood events. Both Macdonald et al. (2014) and Engeland et al. (2018) show that the information content is low when the threshold for historical floods is too low.

In a final step we used the flood rate from the sediment core as a key to explore non-stationarity of the design flood estimates, exemplified by the 200-years flood (Fig. 16). We could see important variation during the recent 6000 years. The 200 years flood was estimated to be around 23 % higher during the flood rich periods in the 18th century and 20% lower during the warmest period. The high values for the 200-years flood during the 18th century is confirmed by the historical data. This variation in design floods is, interestingly within the range seen in recent studies on climate change impacts on floods in Norway (Lawrence, 2020). For a future climate that is expected to be warmer, the design flood might be expected to decrease. Furthermore, this shows that the most interesting information we could get from the sediment core was the non-stationarity in floods.

6.0 Conclusions

In this study we have (i) compiled historical flood data from existing literature, (ii) presented an analysis of sediment core extracted from the lake Flyginnsjøen in Norway including results of XRF- and CT-scans plus MS measurements and used these data to estimate flood frequency over a period of 10 300 years, and (iii) combined flood data from systematic streamflow

measurements, historical sources and lacustrine sediment cores for estimating design floods and assessing non-stationarities in flood frequency at Elverum in the Glomma catchment located in eastern Norway. Our results show that

- Based on detailed analysis of lake sediments that trap sediments whenever the river Glomma exceeds a local threshold, we could estimate flood frequency in a moving window of 50 years throughout the last 10 300 years.

- The paleodata shows that the flood frequency is non-stationary across time scales. Flood rich periods has been identified, and these periods corresponds well to similar data in eastern Norway and also in the Alps such as the increase around 4000 years ago. The flood frequency can show significant non-stationarities within a flood rich period. The most recent period with a high flood frequency was the 18th century, and the 1789 flood (*Stor-Ofsen*) is probably the largest flood during the entire Holocene.

- The estimation of flood quantiles benefits from the use of historical and paleo data. The paleodata were in particular useful for evaluating the historical data. We identified that the 1789 flood was the largest one for the recent 10 300 years and that the 18th century was a flood rich period as compared to the 20th and 19th centuries. Using the frequency of floods obtained from the paleo-flood record resulted in minor changes in design flood estimates.

- We could use the paleodata to explore non-stationarity in design flood estimates. During the coldest period in the 18th century, the design flood was up to 23 % higher than today, and down to 30% lower in a warmer climate c. 4000-6000 years ago.

This study has demonstrated the usefulness of paleo-flood data and we suggest that paleodata has a high potential for detecting links between climate dynamics and flood frequency. The data presented in this study could be used alone, or in combination with paleo-flood data from other locations in Norway and Europe, to analyze the links between changes in climate and its variability and flood frequency.

Data availability

Systematic flood data are available from the national hydrological database at the Norwegian Water Resources and Energy Directorate. The data from the scanning of the sediment cores are available upon request to the authors.

Author contribution

The study was designed and planned by AA, KE, IS and ES. IS and ES carried out the lake coring and the field work. AA, IS. ØP, and ES all contributed the scanning and analysis if the sediment cores. AA, KE and ES contributed to systematization of historical and systematic flood data and the flood frequency analysis. AA prepared Figure 1 and 3 ES and ØP prepared Figure 4. ES prepared Figure 5, 9, 10, 11 and 18. KE prepared Figure 2, 6, 7, 8, 12, 13, 14, 15, 16, and 17. KE prepared the manuscript with contribution from all co-authors.

Competing interests

The authors declare that they have no conflict of interest.

Norway. All core samples, apart from the dating, were measured at the Earth Surface Sediment Laboratory (EARTHLAB) (226171) at Department of Earth Science, University of Bergen.

7 References

Aano, A.: Flood frequency analyses based on streamflow time series, historical information and paleohydrological data., 2017.

Alfieri, L., Bisselink, B., Dottori, F., Naumann, G., de Roo, A., Salamon, P., Wyser, K. and Feyen, L.: Global projections of river flood risk in a warmer world, Earth's Future, 5(2), 171–182, doi:10.1002/2016EF000485, 2017.

Appleby, P. G.: Chronostratigraphic Techniques in Recent Sediments, in Tracking Environmental Change Using Lake Sediments, pp. 171–203, Kluwer Academic Publishers., 2001.

Appleby, P. G. and Piliposian, G. T.: Radiometric Dating of Lake Sediment Cores from Flyginnsjøen and Vingersjøen, Southern Norway (provisional report), Liverpool., 2014.

Baker, V. R.: Paleohydrology and sedimentology of lake missoula flooding in Eastern Washington, Special Paper of the Geological Society of America, 144, 1–73, doi:10.1130/SPE144-p1, 1973.

Baker, V. R.: Paleoflood hydrology and extraordinary flood events, Journal of Hydrology, 96(1–4), 79–99, doi:10.1016/0022-1694(87)90145-4, 1987.

Baker, V. R.: Paleoflood hydrology: Origin, progress, prospects, Geomorphology, 101(1–2), 1–13, doi:10.1016/j.geomorph.2008.05.016, 2008.

Benito, G. and O'Connor, J. E.: Quantitative Paleoflood Hydrology, in Treatise on Geomorphology, vol. 9, pp. 459–474., 2013.

Benito, G. and Thorndycraft, V. R.: Palaeoflood hydrology and its role in applied hydrological sciences, Journal of Hydrology, 313(1–2), 3–15, doi:10.1016/j.jhydrol.2005.02.002, 2005.

Benito, G., Brázdil, R., Herget, J. and Machado, M. J.: Quantitative historical hydrology in Europe, Hydrology and Earth System Sciences, 19(8), 3517–3539, doi:10.5194/hess-19-3517-2015, 2015.

Benson, M. A.: Use of historical data in flood-frequency analysis, Eos, Transactions American Geophysical Union, 31(3), 419–424, doi:10.1029/TR031i003p00419, 1950.

Blaauw, M. and Christeny, J. A.: Flexible paleoclimate age-depth models using an autoregressive gamma process, Bayesian Analysis, 6(3), 457–474, doi:10.1214/11-BA618, 2011.

Blake, G. R. and Hartge, K. H.: Bulk Density, in Methods of Soil Analysis: Part 1—Physical and Mineralogical Methods, edited by K. A, pp. 363–375, American Society of Agronomy-Soil Science Societey of America, Madison., 1986.

Blöschl, G., Hall, J., Parajka, J., Perdigão, R. A. P., Merz, B., Arheimer, B., Aronica, G. T., Bilibashi, A., Bonacci, O., Borga, M., Čanjevac, I., Castellarin, A., Chirico, G. B., Claps, P., Fiala, K., Frolova, N., Gorbachova, L., Gül, A., Hannaford, J., Harrigan, S., Kireeva, M., Kiss, A., Kjeldsen, T. R., Kohnová, S., Koskela, J. J., Ledvinka, O., Macdonald, N., Mavrova-Guirguinova, M., Mediero, L., Merz, R., Molnar, P., Montanari, A., Murphy, C., Osuch, M., Ovcharuk, V., Radevski, I., Rogger, M., Salinas, J. L., Sauquet, E., Šraj, M., Szolgay, J., Viglione, A., Volpi, E., Wilson, D., Zaimi, K. and Živković, N.: Changing climate shifts timing of European floods, Science, 357(6351), 588–590, doi:10.1126/science.aan2506, 2017.

Blöschl, G., Hall, J., Viglione, A., Perdigão, R. A. P., Parajka, J., Merz, B., Lun, D., Arheimer, B., Aronica, G. T., Bilibashi, A., Boháč, M., Bonacci, O., Borga, M., Čanjevac, I., Castellarin, A., Chirico, G. B., Claps, P., Frolova, N., Ganora, D., Gorbachova, L., Gül, A., Hannaford, J., Harrigan, S., Kireeva, M., Kiss, A., Kjeldsen, T. R., Kohnová, S., Koskela, J. J., Ledvinka, O., Macdonald, N., Mavrova-Guirguinova, M., Mediero, L., Merz, R., Molnar, P., Montanari, A., Murphy, C., Osuch, M., Ovcharuk, V., Radevski, I., Salinas, J. L., Sauquet, E., Šraj, M., Szolgay, J., Volpi, E., Wilson, D., Zaimi, K. and Živković, N.: Changing climate both increases and decreases European river floods, Nature, 573(7772), 108–111, doi:10.1038/s41586-019-1495-6, 2019.

Bøe, A.-G., Dahl, S. O., Lie, Ø. and Nesje, A.: Holocene river floods in the upper Glomma catchment, southern Norway: a high-resolution multiproxy record from lacustrine sediments, The Holocene, 16, 445–455, doi:10.1191/0959683606hl940rp, 2006.

Brázdil, R., Pfister, C., Wanner, H., von Storch, H. and Luterbacher, J.: Historical climatology in Europe - The state of the art, Climatic Change, 70(3), 363–430, doi:10.1007/s10584-005-5924-1, 2005.

Brázdil, R., Kundzewicz, Z. W. and Benito, G.: Historical hydrology for studying flood risk in Europe, Hydrological Sciences Journal, 51(5), 739–764, doi:10.1623/hysj.51.5.739, 2006a.

Brázdil, R., Kundzewicz, Z. W. and Benito, G.: Historical hydrology for studying flood risk in Europe, Hydrological Sciences Journal, 51(5), 739–764, doi:10.1623/hysj.51.5.739, 2006b.

Brázdil, R., Máčka, Z., Řezníčková, L., Soukalová, E., Dobrovolný, P. and Grygar, T. M.: Floods and floodplain changes of the River Morava, the Strážnické Pomoraví region (Czech Republic) over the past 130 years, Hydrological Sciences Journal, 56(7), 1166–1185, doi:10.1080/02626667.2011.608359, 2011.

Brázdil, R., Kundzewicz, Z. W., Benito, G., Demarée, G., Macdonald, N. and Roald, L. A.: Historical floods in europe in the past millennium, IAHS-AISH Publication, (SPEC. ISS. 10), 121–166, doi:10.1201/b12348-7, 2012.

Bretz, J. H.: Valley Deposits Immediately East of the Channeled Scabland of Washington. I, The Journal of Geology, 37, 393–427, doi:10.2307/30056651, 1929.

Coles, S. G. and Dixon, M. J.: Likelihood-Based Inference for Extreme Value Models, Extremes, 2(1), 5–23, doi:10.1023/A:1009905222644, 1999.

Cunnane, C. Unbiased plotting positions – a review – comments. Journal of Hydrology 37, 205–222. doi:10.1016/ 0022-1694(78)90017-3, 1978

Czymzik, M., Brauer, A., Dulski, P., Plessen, B., Naumann, R., von Grafenstein, U. and Scheffler, R.: Orbital and solar forcing of shifts in Mid- to Late Holocene flood intensity from varved sediments of pre-alpine Lake Ammersee (southern Germany), Quaternary Science Reviews, 61, 96–110, doi:10.1016/j.quascirev.2012.11.010, 2013.

Dana, J. D.: The flood of the Connecticut River valley from the melting of the Quaternary glacier, American Journal of Science, s3-23(134), 87–97, doi:10.2475/ajs.s3-23.134.87, 1882.

Dean, W. E. Jr.: Determination of Carbonate and Organic Matter in Calcareous Sediments and Sedimentary Rocks by Loss on Ignition: Comparison With Other Methods, SEPM Journal of Sedimentary Research, Vol. 44(1), 242–248, doi:10.1306/74d729d2-2b21-11d7-8648000102c1865d, 1974.

Debret, M., Chapron, E., Desmet, M., Rolland-Revel, M., Magand, O., Trentesaux, A., Bout-Roumazeille, V., Nomade, J. and Arnaud, F.: North western Alps Holocene paleohydrology recorded by flooding activity in Lake Le Bourget, France, Quaternary Science Reviews, 29(17–18), 2185–2200, doi:10.1016/j.quascirev.2010.05.016, 2010.

Embrechts, P., Klüppelberg, C. and Mikosch, T.: Modelling Extremal Events, Springer Berlin Heidelberg, Berlin, Heidelberg., 1997.

Engeland, K., Wilson, D., Borsányi, P., Roald, L. and Holmqvist, E.: Use of historical data in flood frequency analysis: A case study for four catchments in Norway, in Hydrology Research, vol. 49, pp. 466–486, Nordic Association for Hydrology., 2018.

Evin, G., Wilhelm B., , Jenny J.P.: Flood hazard assessment of the Rhône River revisited with reconstructed discharges from lake sediments, Global and Planetary Change 172 (114-123) , , 10.1016/j.gloplacha.2018.09.010, 2019

Finne-Grønn, S. H.: Elverum : en bygdebeskrivelse. 2 : Bygdens almindelige historie, institutioner og embedsmænd, Cammenmeyers Boghandel, Oslo. [online] Available from: https://www.nb.no/items/0c92bf63bcd34a40d851ec9aed2d8f07?page=243&searchText=elverum%20en%20bygdebeskrivels e (Accessed 5 March 2020), 1921.

Fisher, R. A. and Tippett, L. H. C.: Limiting forms of the frequency distribution of the largest or smallest member of a sample, Mathematical Proceedings of the Cambridge Philosophical Society, 24(02), 180–190, doi:10.1017/S0305004100015681, 1928.

Follestad, K.: Reconstruction of floods in Glomma through the holos - Effects of climate change on different flood regimes (Rekonstruksjon av flommer i Glomma gjennom holosen - Effekter av klimaendringer på ulike flomregimer - in Norwegian), Bergen. [online] Available from: https://www.uib.no/geografi/83037/rekonstruksjon-av-flommer-i-glomma-gjennom-holosen-effekter-av-klimaendringer-på (Accessed 5 March 2020), 2014.

Gaál, L., Szolgay, J., Kohnová, S., Hlavčová, K. and Viglione, A.: Inclusion of historical information in flood frequency analysis using a Bayesian MCMC technique: a case study for the power dam Orlík, Czech Republic, Contributions to Geophysics and Geodesy, 40, 121–147, doi:10.2478/v10126-010-0005-5, 2010.

Gilli, A., Anselmetti, F. S., Glur, L. and Wirth, S. B.: Lake Sediments as Archives of Recurrence Rates and Intensities of Past Flood Events, in Dating Torrential Processes on Fans and Cones, vol. 47, edited by M. Schneuwly-Bollschweiler, M. Stoffe, and F. Rudolf-Miklau, pp. 225–242, Springer International Publishing., 2013.

Glaser, R., Riemann, D., Schönbein, J., Barriendos, M., Brázdil, R., Bertolin, C., Camuffo, D., Deutsch, M., Dobrovolný, P., van Engelen, A., Enzi, S., Halíčková, M., Koenig, S. J., Kotyza, O., Limanówka, D., Macková, J., Sghedoni, M., Martin, B. and Himmelsbach, I.: The variability of European floods since AD 1500, Climatic Change, 101(1–2), 235–256, doi:10.1007/s10584-010-9816-7, 2010.

GLB: Glommen og Laagens Grukseierforening 1918-43, Grøndahl & Søns Boktrykkeri, Oslo., 1947.

Gnedenko, B.: Sur La Distribution Limite Du Terme Maximum D'Une Serie Aleatoire, The Annals of Mathematics, 44(3), 423, doi:10.2307/1968974, 1943.

Goslar, T.: Poznan Radiocarbon Laboratory, Poland, Poznan., 2014.

Grønlund, A., Njøs, A. and Kløve, B.: Endringer i landbrukets arealbruk i Glommas nedbørfelt, Oslo. [online] Available from: http://publikasjoner.nve.no/hydra/rapport/n02.pdf (Accessed 5 March 2020), 1999.

Hall, J., Arheimer, B., Borga, M., Brázdil, R., Claps, P., Kiss, a., Kjeldsen, T. R., Kriaučiūnienė, J., Kundzewicz, Z. W., Lang, M., Llasat, M. C., Macdonald, N., McIntyre, N., Mediero, L., Merz, B., Merz, R., Molnar, P., Montanari, a., Neuhold, C., Parajka, J., Perdigão, R. a. P., Plavcová, L., Rogger, M., Salinas, J. L., Sauquet, E., Schär, C., Szolgay, J., Viglione, a. and Blöschl, G.: Understanding flood regime changes in Europe: a state-of-the-art assessment, Hydrology and Earth System Sciences, 18(7), 2735–2772, doi:10.5194/hess-18-2735-2014, 2014.

Hanssen-Bauer, I. Førland, E. J. Haddeland, I., Hisdal, H., Lawrence, D., Mayer, S., Nesje, A., Sandven, J. E. Ø., Sandø, A. B. and Sorteberg, A. Ådlandsvik, B.: Climate in Norway 2100: a knowledge based for climate adaptation., 2017.

Hegge, K.: Glommas Bifurkasjon Ved Kongsvinger, Norsk Geografisk Tidsskrift, 22(2), 166–171, doi:10.1080/00291956808551859, 1968.

Hegge, K.: Large floods in Glomma (Store flommer i Glomma - in Norwegian), , 2, 1969.

Hirabayashi, Y., Mahendran, R., Koirala, S., Konoshima, L., Yamazaki, D., Watanabe, S., Kim, H. and Kanae, S.: Global flood risk under climate change, Nature Climate Change, 3(9), 816–821, doi:10.1038/nclimate1911, 2013.

Hirsch, R. M. & Stedinger, J. R. Plotting positions for historical floods and their precision. Water Resources Research 23 (4), 715–727. doi:10.1029/WR023i004p00715, 1987

Høgaas, F. and Longva, O.: Mega deposits and erosive features related to the glacial lake Nedre Glomsjø outburst flood, southeastern Norway, Quaternary Science Reviews, 151, 273–291, doi:10.1016/j.quascirev.2016.09.015, 2016.

IPCC: Managing the Risks of Extreme Events and Disasters to Advance Climate Change Adaptation — IPCC, edited by C. B. Field, V. Barros, T. F. Stocker, D. Qin, D. J. Dokken, K. L. Ebi, M. D. Mastrandrea, K. J. Mach, G.-K. Plattner, S. K. Allen, M. Tignor, and P. M. Midgley, Cambridge University Press. [online] Available from: https://www.ipcc.ch/report/managing-the-risks-of-extreme-events-and-disasters-to-advance-climate-change-adaptation/ (Accessed 4 March 2020), 2012.

Jacobeit, J., Glaser, R., Luterbacher, J. and Wanner, H.: Links between flood events in central Europe since AD 1500 and large-scale atmospheric circulation modes, Geophysical Research Letters, 30(4), 2–5, doi:10.1029/2002GL016433, 2003.

Killingland, K. E. N.: Extreme floods in Grimsa, upper Glomma. Reconstruction of flood frequency through holocene and vulnerability analysis of today's river (Ekstremflommer i Grimsa, øvre Glommavassdraget Rekonstruksjon av flomfrekvens gjennom holosen og sårbarhetsanalyse av d, The University of Bergen., 2009.

Kjeldsen, T. R., Macdonald, N., Lang, M., Mediero, L., Albuquerque, T., Bogdanowicz, E., Braˊzdil, R., Castellarin, A., David, V., Fleig, A., Gu¨l, G. O., Kriauciuniene, J., Kohnovaˊ, S., Merz, B., Nicholson, O., Roald, L. A., Salinas, J. L., Sarauskiene, D., Sˇraj, M., Strupczewski, W., Szolgay, J., Toumazis, A., Vanneuville, W., Veijalainen, N. and Wilson, D.: Documentary evidence of past floods in Europe and their utility in flood frequency estimation, Journal of Hydrology, 517, 963–973, doi:10.1016/j.jhydrol.2014.06.038, 2014.

Klæboe, H.: Glommas bifurkasjon ved kongsvinger, Norsk Geografisk Tidsskrift, 11(5–6), 266–275, doi:10.1080/00291954608551633, 1946.

Kochel, R. C. and Baker, V. R.: Paleoflood hydrology, Science, 215(4531), 353–361, doi:10.1126/science.215.4531.353, 1982.

Koh, H. M., Park, W. and Choo, J. F.: Lifetime design of long-span bridges, Structure and Infrastructure Engineering, 10(4), 521–533, doi:10.1080/15732479.2013.769013, 2014.

Kundzewicz, Zbigniew. and International Association of Hydrological Sciences.: Changes in flood risk in Europe, International Association of Hydrological Sciences., 2012.

Kvernmoen, G. T. and Kvernmoen, T.: Flomopptegnelser (1740-1839), in Elverum – en bygdebeskrivelse –II – Bygdens almenne historie», edited by S. H. Finne-Grønn, Oslo., 1921.

Kvisvik, B. C., Paasche, Ø. and Dahl, S. O.: Holocene cirque glacier activity in Rondane, southern Norway, Geomorphology, 246, 433–444, doi:10.1016/j.geomorph.2015.06.046, 2015.

Lawrence, D.: Uncertainty introduced by flood frequency analysis in projections for changes in flood magnitudes under a future climate in Norway, Journal of Hydrology: Regional Studies, 28, 100675, doi:10.1016/j.ejrh.2020.100675, 2020.

Lovdata: Dam Safety Regulation (Forskrift om sikkerhet ved vassdragsanlegg, in Norwegian). [online] Available from: https://lovdata.no/dokument/SF/forskrift/2009-12-18-1600?q=damsikkerhet (Accessed 5 March 2020), 2010.

Macdonald, N. and Sangster, H.: High-magnitude flooding across Britain since AD 1750, Hydrology and Earth System Sciences, 21(3), 1631–1650, doi:10.5194/hess-21-1631-2017, 2017.

Macdonald, N., Kjeldsen, T. R., Prosdocimi, I. and Sangster, H.: Reassessing flood frequency for the Sussex Ouse, Lewes: the inclusion of historical flood information since AD 1650, Natural Hazards and Earth System Sciences, 14(10), 2817–2828, doi:10.5194/nhess-14-2817-2014, 2014.

Martins, E. S. and Stedinger, J. R.: Generalized maximum-likelihood generalized extreme-value quantile estimators for hydrologic data, Water Resources Research, 36(3), 737–744, doi:10.1029/1999WR900330, 2000.

Martins, E. S. and Stedinger, J. R.: Historical information in a generalized maximum likelihood framework with partial duration and annual maximum series, Water Resources Research, 37(10), 2559–2567, doi:10.1029/2000WR000009, 2001.

Milly, P. C. D., Betancourt, J., Falkenmark, M., Hirsch, R. M., Kundzewicz, Z. W., Lettenmaier, D. P. and Stouffer, R. J.: Stationarity Is Dead: Whither Water Management?, Science, 319(5863), 573–574, doi:10.1126/science.1151915, 2008.

Moberg, A., Sonechkin, D. M., Holmgren, K., Datsenko, M. H. and Karlén, W.: Highly variable Northern Hemisphere temperatures reconstructed from low- and high-resolution proxy data, Nature, 433(7026), 613–617, doi:10.1038/nature03265, 2005.

Mudelsee, M., Börngen, M., Tetzlaff, G. and Grünewald, U.: Extreme floods in central Europe over the past 500 years: Role of cyclone pathway "Zugstrasse Vb," Journal of Geophysical Research D: Atmospheres, 109(23), 1–21, doi:10.1029/2004JD005034, 2004.

Nesje, A.: A piston corer for lacustrine and marine sediments, Arctic and Alpine Research, 24(3), 257–259, doi:10.2307/1551667, 1992.

Nesje, A., Dahl, S. O., Matthews, J. A. and Berrisford, M. S.: A ~4500 yr record of river floods obtained from a sediment core in Lake Atnsjøen, eastern Norway, Journal of Paleolimnology, 25(3), 329–342, doi:10.1023/A:1011197507174, 2001.

NVE flood zone maps: NVE flood zone maps, [online] Available from: https://gis3.nve.no/link/?link=flomsone (Accessed 23 May 2020), 2020.

Orvedal, K. and Peereboom, I. O.: Flood zone map Førde (Flaumsonekart Delprosjekt Førde - in Norwegian)., 2014.

Otnes, J.: Old floodmarks at River Glomma (Gamle flommerker langs Glåma, Årbok for Glåmdalen 41, 6–26), Elverum Trykk, Elverum., 1982.

Paasche, Ø. and Støren, E. W. N.: How Does Climate Impact Floods? Closing the Knowledge Gap, Eos, Transactions American Geophysical Union, 95(28), 253–254, doi:10.1002/2014EO280001, 2014.

Payrastre, O., Gaume, E. and Andrieu, H.: Usefulness of historical information for flood frequency analyses: Developments based on a case study, Water Resources Research, 47, doi:10.1029/2010WR009812, 2011.

Pettersson, L.-E.: Flood estimation for the Glomma river upstream Vorma (Flomberegning for Glommavassdraget oppstrøms Vorma - in Norwegian), Oslo. [online] Available from: www.nve.no (Accessed 5 March 2020), 2000.

Pettersson, L.-E.: Glomma's bifucation at Kongsvinger (Glommas bifurkasjon ved Kongsvinger - in Norwegian), Oslo. [online] Available from: www.nve.no (Accessed 5 March 2020), 2001.

Prosdocimi, I.: German tanks and historical records: the estimation of the time coverage of ungauged extreme events, Stochastic Environmental Research and Risk Assessment, 32(3), 607–622, doi:10.1007/s00477-017-1418-8, 2018.

Reimer, P. J., Bard, E., Bayliss, A., Beck, J. W., Blackwell, P. G., Ramsey, C. B., Buck, C. E., Cheng, H., Edwards, R. L., Friedrich, M., Grootes, P. M., Guilderson, T. P., Haflidason, H., Hajdas, I., Hatté, C., Heaton, T. J., Hoffmann, D. L., Hogg, A. G., Hughen, K. A., Kaiser, K. F., Kromer, B., Manning, S. W., Niu, M., Reimer, R. W., Richards, D. A., Scott, E. M., Southon, J. R., Staff, R. A., Turney, C. S. M. and van der Plicht, J.: IntCal13 and Marine13 Radiocarbon Age Calibration Curves 0–50,000 Years cal BP, Radiocarbon, 55(4), 1869–1887, doi:10.2458/azu_js_rc.55.16947, 2013.

Renard, B., Sun, X. and Lang, M.: Bayesian Methods for Non-stationary Extreme Value Analysis, pp. 39–95., 2013.

Renberg, I. and Hansson, H.: The HTH sediment corer, Journal of Paleolimnology, 40(2), 655–659, doi:10.1007/s10933-007-9188-9, 2008.

Reusch, H.: Glomma's bend at Kongsvinger (Glommens bøining ved Kongsvinger), in Norges Geografiske Selskab, Aarbog, 14, pp. 96–102., 1903.

Roald, L.: Floods in Norway (Flom i Norge - in Norwegian), Forlaget Tom & Tom, Oslo., 2013.

Schendel, T. and Thongwichian, R.: Considering historical flood events in flood frequency analysis: Is it worth the effort?, Advances in Water Resources, 105, 144–153, doi:10.1016/j.advwatres.2017.05.002, 2017.

Schillereff, D. N., Chiverrell, R. C., Macdonald, N. and Hooke, J. M.: Flood stratigraphies in lake sediments: A review, Earth-Science Reviews, 135, 17–37, doi:10.1016/j.earscirev.2014.03.011, 2014.

Schubert,A., Lauterbach,S., Leipe,C., Scholz,V., Brauer,A., Tarasov,P.E.Anthropogenic and climate controls on vegetation changes between 1500 BCE and 500 CE reconstructed from a high-resolution pollen record from varved sediments of Lake Mondsee, Austria, Palaeogeography, Palaeoclimatology, Palaeoecology (559) https://doi.org/10.1016/j.palaeo. 2020.109976 2020

Serinaldi, F. and Kilsby, C. G.: Stationarity is undead: Uncertainty dominates the distribution of extremes, Advances in Water Resources, 77, 17–36, doi:10.1016/j.advwatres.2014.12.013, 2015.

Stedinger, J. R. and Cohn, T. A.: Flood Frequency Analysis With Historical and Paleoflood Information, Water Resources Research, 22(5), 785–793, doi:10.1029/WR022i005p00785, 1986.

Steffensen, I. G.: Reconstruction of large floods in Glomma through the Holocene - possible links to natural climate variability and global atmospheric circulation (Rekonstruksjon av storflommer i Glomma gjennom holosen-mulige koblinger til naturlig klimavariabilitet og global atmosfaerisk sirkulasjon - in Norwegian), The University of Bergen, Bergen, 15 May., 2014.

Støren, E. N. and Paasche, Ø.: Scandinavian floods: From past observations to future trends, Global and Planetary Change, 113, 34–43, doi:10.1016/j.gloplacha.2013.12.002, 2014.

Støren, E. N., Dahl, S. O., Nesje, A. and Paasche, Ø.: Identifying the sedimentary imprint of high-frequency Holocene river floods in lake sediments: development and application of a new method, Quaternary Science Reviews, 29(23–24), 3021–3033, doi:10.1016/j.quascirev.2010.06.038, 2010.

Støren, E. N., Kolstad, E. W. and Paasche, Ø.: Linking past flood frequencies in Norway to regional atmospheric circulation anomalies, Journal of Quaternary Science, 27(1), 71–80, doi:10.1002/jqs.1520, 2012.

Støren, E. W. N., Paasche, Ø., Hirt, A. M. and Kumari, M.: Magnetic and geochemical signatures of flood layers in a lake system, Geochemistry, Geophysics, Geosystems, 17(10), 4236–4253, doi:10.1002/2016GC006540, 2016.

Swierczynski, T., Lauterbach, S., Dulski, P., Delgado, J., Merz, B. and Brauer, A.: Mid- to late Holocene flood frequency changes in the northeastern Alps as recorded in varved sediments of Lake Mondsee (Upper Austria), Quaternary Science Reviews, 80, 78–90, doi:10.1016/j.quascirev.2013.08.018, 2013.

Tarr, R. S.: A hint with respect to the origin of terraces in glaciated regions, American Journal of Science, s3-44(259), 59–61, doi:10.2475/ajs.s3-44.259.59, 1892.

TEK17: Building regulations (Byggtekninsk forskrift TEK17 - in Norwegian). [online] Available from: https://dibk.no/byggereglene/byggteknisk-forskrift-tek17/7/7-2/, 2018.

Velle, G., Bjune, A. E., Larsen, J. and Birks, H. J. B.: Holocene climate and environmental history of Brurskardstjørni, a lake in the catchment of Øvre Heimdalsvatn, south-central Norway, Hydrobiologia, 642(1), 13–34, doi:10.1007/s10750-010-0153-7, 2010.

Viglione, A.: nsRFA: Non-supervised Regional Frequency Analysis. R package version 0.7-11., [online] Available from: http://cran.r-project.org/package=nsRFA, 2012.

Viglione, A., Merz, R., Salinas, J. L. and Blöschl, G.: Flood frequency hydrology: 3. A Bayesian analysis, Water Resources Research, 49(2), 675–692, doi:10.1029/2011WR010782, 2013.

Vormoor, K., Lawrence, D., Schlichting, L., Wilson, D. and Wong, W. K.: Evidence for changes in the magnitude and frequency of observed rainfall vs. snowmelt driven floods in Norway, Journal of Hydrology, 538, 33–48, doi:10.1016/j.jhydrol.2016.03.066, 2016.

Walker, M., Johnsen, S., Rasmussen, S. O., Popp, T., Steffensen, J.-P., Gibbard, P., Hoek, W., Lowe, J., Andrews, J., Björck, S., Cwynar, L. C., Hughen, K., Kershaw, P., Kromer, B., Litt, T., Lowe, D. J., Nakagawa, T., Newnham, R., and Schwander, J. Formal definition and dating of the GSSP (Global Stratotype Section and Point) for the base of the Holocene using the Greenland NGRIP ice core, and selected auxiliary records. J. Quaternary Sci ., Vol. 24 pp. 3–17. ISSN 0267-8179, 2009

Wellington, S. L. and Vinegar, H. J.: X-RAY COMPUTERIZED TOMOGRAPHY., JPT, Journal of Petroleum Technology, 39(8), 885–898, doi:10.2118/16983-PA, 1987.

Wilhelm, B., Ballesteros Canovas, J. A., Corella Aznar, J. P., Kämpf, L., Swierczynski, T., Stoffel, M., Støren, E. and Toonen, W.: Recent advances in paleoflood hydrology: From new archives to data compilation and analysis, Water Security, 3(May), 1–8, doi:10.1016/j.wasec.2018.07.001, 2018.

Wirth, S. B., Glur, L., Gilli, A. and Anselmetti, F. S.: Holocene flood frequency across the Central Alps - solar forcing and evidence for variations in North Atlantic atmospheric circulation, Quaternary Science Reviews, 80, 112–128, doi:10.1016/j.quascirev.2013.09.002, 2013.

Østmoe, A. The Large flood of 1789: the weather system that led to the largest flood disaster in Norway (Stor-ofsen 1789 : værsystemet som førte til den største flomkatastrofen i Norge - in Norwegian), Oversiktsregisteret, Ski, Norway, 1985